TÉCNICO LISBOA

Computational Modelling of Flatfoot Deformity

Mariana Rocha Alves

Thesis to obtain the Master of Science Degree in

Biomedical Engineering

Supervisors: Prof. Paulo Rui Alves Fernandes

Prof. João Orlando Maques Gameiro Folgado

Examination Committee

Chairperson: Prof. João Miguel Raposo Sanches

Supervisor: Prof. Paulo Rui Alves Fernandes

Members of the Committee: Prof. Carlos Miguel Fernandes Quental

Dr. João Vide

December 2020

Preface

The work presented in this thesis was performed at the Mechanical Engineer Department (DEM) of Instituto Superior Técnico (Lisbon, Portugal), during the period March-December 2020, under the supervision of Prof. Paulo Fernandes and Prof. João Folgado.

Declaration

I declare that this document is an original work of my own authorship and that it fulfils all the requirements of the Code of Conduct and Good Practices of the Universidade de Lisboa.

Acknowledgments

Porque ninguém faz nada sozinho, no fim deste percurso, resta-me agradecer. Em primeiro lugar, aos meus orientadores Prof. Paulo Fernandes e Prof. João Folgado, pelo acompanhamento prestado ao longo dos últimos meses. Ao Prof. André, que apesar de não ser meu orientador, revelou-se sempre pronto a ajudar.

Agradeço também ao Dr. João Vide e ao Dr. Afonso Cardoso, dos quais partiu a ideia para o tema da dissertação, pelo acompanhamento médico prestado.

Aos meus amigos de sempre. Foi com eles que cheguei até aqui e, apesar dos percursos diferentes que cada um tomou, sabemos que é entre nós que encontramos a verdadeira amizade. Á melhor coisa que o Técnico me deu, a minha amiga Isabel, companheira de todas as horas, com a qual vivi os melhores e piores momentos da faculdade, mas juntas sabiamos sempre que iria dar certo.

Ao meu tio e padrinho Vasco, o meu grande obrigada, por me ter proporcionado o espaço que tive o privilégio de chamar casa durante estes 5 anos e por me ter feito sempre sentir em casa com as suas visitas frequentes a Lisboa nas quais vivemos experiências (gastronómicas, principalmente) fantásticas.

Ás minhas avós, avó da Praia e avó das Patas, que com a sua voz e coração doce que caracterizam as avós, telefonavam com frequência, para fazer diminuir a distância que nos separava.

Ao meu namorado, João, que apesar de não me ter acompanhado em todo o percurso no Técnico, foi um apoio crucial nos últimos 2 anos. Fez-me sempre acreditar no meu valor, deu-me muito carinho e momentos muito felizes no Porto, em Lisboa e na Terceira, que ajudavam a recarregar energias para continuar.

Por fim, o maior dos agradecimentos, aos meus pais, que são os melhores do mundo, que durante toda a minha vida nunca deixaram que me faltasse nada e que, com o coração apertado, me deram a oportunidade de sair do conforto de casa para me tornar Engenheira Biomédica. Permitiram sempre que eu trilhasse o meu próprio caminho e apoiaram-me em todos os obstáculos que foram aparecendo. Um obrigada especial ao meu irmão João Pedro, o grande amor da minha vida e meu maior orgulho, por me olhar sempre com admiração e por me proporcionar o amor mais puro que existe que é o amor de irmãos.

À minha ilha Terceira, o pequeno pedaço de terra que irei sempre chamar de casa, que durante estes 5 anos, foi o meu refúgio e onde vivi momentos muito felizes junto da minha família e amigos.

Por fim, agradeço ao Insitituto Superior Técnico, esta casa de excelência que me acolheu, por todo o conhecimento adquirido e pela capacidade de desenrasque incrível que caracteriza um verdadeiro Engenheiro.

Abstract

Flatfoot is a deformity that leads to the misalignment of the foot and ankle joints, affecting 25% of the general population. Despite being a common foot deformity, the biomechanics of flatfoot are not fully understood. Choosing the best suited surgical treatment to correct this deformity is a troubling subject among the medical community. This work is presented as a first approach, using Finite Element Method for the evaluation of the biomechanical behaviour of the foot when its anatomy sets up in a valgus foot situation. A foot and ankle finite element model of both a healthy and a flatfoot were developed consisting of bones, cartilages, ligaments, and tendons. A comparison between the von Mises stresses distribution of the healthy and the flatfoot was performed. Overall, the results showed that the flatfoot was subjected to higher stresses than the healthy foot. The cartilages and ligaments of the flatfoot also yield higher stresses than the healthy foot. The clinical use of this type of FE models can be of great importance since they can lead the way for novel diagnostic techniques and novel methods for treatment planning/optimization. In the future, a study of which should be the most suitable osteotomy for flatfoot correction will be performed, using the model developed in this work.

Keywords: Flatfoot, Finite Element Method, Ligaments, Biomechanics

Resumo

O pé plano é uma deformação que leva ao mau alinhamento das articulações do pé e tornozelo que afecta cerca de 25% da população global. Apesar de ser uma deformação comum, a sua biomecânica não é totalmente conhecida. O vasto leque de tratamentos disponíveis para a correcção desta deformação, leva a que não exista um consenso na comunidade médica de qual o tratamento que melhor restabelece a função biomecânica do pé. Este trabalho apresenta-se como uma primeira abordagem, utilizando o Método dos Elementos Finitos, para a avaliação das alterações biomecânicas envolvidas na deformação do pé plano, comparativamente a um pé saudável. Para isso, foi desenvolvido um modelo de elementos finitos de um pé saudável e de um pé plano, constituído por ossos, cartilagens, ligamentos e tendões. A comparação entre o pé saudável e o pé plano foi feita através do estudo da distribuição das tensões de von Mises nos dois modelos. No geral, os resultados mostraram que o pé plano está sujeito a maiores valores de tensão. No caso das cartilagens e dos ligamentos/tendões, também se obtiveram valores de tensão mais elevados para o caso do pé plano. Este tipo de modelos de elementos finitos pode ter grande utilidade quando incorporado na prática clínica, surgindo como uma ferramenta de apoio à decisão e planeamento cirúrgico. Futuramente, esta estratégia será aplicada no estudo computacional das osteotomias, visto que se pretende obter indicações de qual a técnica de ostetomia mais indicada na restauração da função normal do pé.

Palavras-chave: Pé Plano, Método dos Elementos Finitos, Ligamentos, Biomecânica

Contents

Introduction 1

1.1. Motivation 1

1.2. Thesis Outline 2

Background 3

2.1. Terminology 3

2.1.1. Anatomical Reference Position 3

2.1.2. Anatomical Reference Planes and Axes 3

2.1.3. Motion Terminology 4

2.2. Foot and Ankle Anatomy 5

2.2.1. Bones 5

2.2.2. Joints and Ligaments 7

2.2.3. Muscles 10

2.2.4. Foot Arches 11

2.3. Valgus Foot 12

2.3.1. Etiology and Classification 12

2.3.2. Diagnosis 14

2.3.3. Treatment 15

2.4. Finite Element Foot and Ankle Models 16

Methods 20

3.1. Image Acquisition and Segmentation 20

3.2. Cartilage Modelling 23

3.3. FE Modelling 24

3.3.1. Ligament Insertion 24

3.3.2. Material Properties 26
3.3.3. Model Interactions 28
3.3.4. Loading and Boundary Conditions 28
3.3.5. Mesh Generation 29
Results and Discussion 30
4.1. Bones and cartilages 30
4.2. Ligaments and Tendons 37
Conclusion 39
5.1. Limitations and Future Work 39
References 41

List of Tables

Table 1 - Extrinsic muscles of foot and ankle complex. (Adapted from [6]) 10

Table 2 - Intrinsic muscles of the foot and ankle complex .(Adapted from [6]) 11

Table 3 - Myerson Modification of Johnson and Storm Classification of Adult-Acquired Flatfoot Deformity. (Adapted from [12]) 13

Table 4 - Material properties for ligaments and tendons.....27

List of Figures

Figure 1 – Anatomical reference planes and corresponding axis (a) applied to the human body and (b) applied to foot and ankle complex. (Adapted from [3],[5])....4

Figure 2 - Movements of foot and ankle (a) in the sagittal plane: dorsiflexion and plantar flexion, (b) in the axial plane: abduction (left) and adduction (right), (c) in the coronal plane: eversion (left) and inversion (right) and (d) involving the 3 anatomical reference planes: pronation (left) and supination (right). These figures represent right foot (Adapted from [3])....5

Figure 3 - Foot bones: (a): Division of the foot into the three bony groups (b): Bony structure of the foot. Both figures represent a superiorly vision of the right foot. (Adapted from [6])....7

Figure 4 - (a) Anterior view of the ankle joint with the foot plantarflexed, (b) deltoid ligament and (c) lateral ligaments. All the figures represent the right foot. (Adapted from [6])....8

Figure 5 - Tarsometatarsal, metatarsophalangeal, and interphalangeal joints, right foot. (Adapted from [6])....10

Figure 6 - Foot arches. (a) - longitudinal arches: medial arch (on top) and lateral arch (on the bottom) and (b) – transverse arch. Both images represent the right foot. (Adapted from [5])....12

Figure 7 - Alignment of the foot joints in (a) normal foot and (b) flatfoot. The coloured lines represent the arches of the foot. (Adapted from [10])....13

Figure 8 -(a) Ankle model developed by Patil et al. (Adapted from [15]) and (b) 3-D ankle model created by Jacob et al. (Adapted from [16])....17

Figure 9 -(a) Bony structure of the model created by Cheung et al. and (b) FE model of the soft tissue capsule. (Adapted from [19])....18

Figure 10 - Labels used to identify different regions on the segmentation. 21

Figure 11 - ROI (in red) for the active contour segmentation of the calcaneus bone: (a) axial view , (b) coronal view and (c) sagittal view....21

Figure 12 - Axial view of the evolution of the active contour method of the calcaneus bone for (a) t=0, (b) t=50, (c) t=100, (d) t=200 and (e) t=400 and sagittal view of the 3D evolution of the active contour method of the calcaneus bone for (f) t=0, (g) t=50, (h) t=100, (i) t=200 and (j) t=400. 22

Figure 13 - Final segmentation of foot bones after active contour and manual segmentation methods performed in ITK-SNAP....22

Figure 14 – Imported mesh surface of calcaneus bone of the healthy foot model from ITK-SNAP to MeshLab. (a) without Laplacian smoothing filtering and (b) with Laplacian smoothing filtering.....23

Figure 15 -3D foot models after inserting cartilages with the bones coloured grey and the cartilages in red - (a): normal foot and (b): valgus foot.....24

Figure 16 – FE models of the foot and ankle comprising bones, cartilages and ligaments. (a) and (b) normal foot: (a) – lateral view and (b) – plantar view. (c) and (d) valgus foot: (c) – lateral view and (d) – plantar view. 25

Figure 17 -TPT in its right position after creating a datum axis (dashed yellow lines) with 2 points, applying a parallel edge constraint and translating the tendon to its final position.....26

Figure 18 – Loading conditions applied to the normal foot. (a) RP on the top of the tibia surface where the load was applied and (b) Surface (highlighted in red) that was coupled to the RP for distributing the load. 28

Figure 19 - Boundary conditions applied on the healthy foot. 28

Figure 20 - Meshed foot models. (a) Mesh generated on the normal foot and (b) mesh generated on flatfoot.....29

Figure 21 - Von Mises stresses distribution on the healthy foot. (a) lateral view, (b) medial view, (c) posterior view, (d) frontal view and (e) plantar view. 30

Figure 22 - Von Mises stresses distribution on the flatfoot. (a) lateral view, (b) medial view, (c) posterior view, (d) frontal view and (e) plantar view. 31

Figure 23 – von Mises stresses on the calcaneus bone for healthy foot. (a) medial view, (b) lateral view and (c) plantar view. 32

Figure 24 – von Mises stresses on the calcaneus bone for the flatfoot. (a) medial view, (b), lateral view and (c) plantar view. 33

Figure 25 – von Mises stresses distribution on the talus bone for the healthy foot. (a) medial view, (b) lateral view, (c) plantar view and (d) superior view. 33

Figure 26 – von Mises stresses distribution on the talus bone for the flatfoot. (a) medial view, (b) lateral view, (c) plantar view and (d) superior view. 34

Figure 27 – von Mises stresses distribution on the tibia for the healthy foot. (a) anterior view, (b) posterior view and (c) inferior view. 35

Figure 28 – von Mises stresses distributions on tibia for the flatfoot. (a) anterior view, (b) posterior view and (c) inferior view. 35

Figure 29 – von Mises stresses distribution on fibula for the healthy foot. (a) lateral view and (b) medial view. 35

Figure 30 -von Mises stresses distribution on fibula for the flatfoot. (a) lateral view and (b) medial view. 36

Figure 31 -von Mises peak stresses acting on the cartilages for the healthy foot (blue) and for the flatfoot (grey). 36

Figure 32 –(a) Long Plantar Ligament divided into its 5 parts and (b) TPT divided in its 2 parts. 37

Figure 33 – Ligaments and tendons stresses acting on the healthy foot (blue) and on the flatfoot (grey). 38

Acronyms

AAFD Acquired Flatfoot Deformity

AT Achilles Tendon

ATi Anterior Tibiotalar

DL Deltoid Ligament

FE Finite Element

FEM Finite Element Method

LPL Long Plantar Ligament

PTi Posterior Tibiotalar

ROI Region of Interest

SL Spring Ligament

SPL Short Plantar Ligament

TC Tibiocalcaneal

TN Tibionavicular

TPT Tibialis Posterior Tendon

Nomenclature

$\boldsymbol{E}$	Young's Modulus
υ	Poisson's Ratio

Chapter 1

Introduction

Throughout this chapter the work motivation is described, the goals are established, and the structure of the thesis document is explained.

1.1. Motivation

Flatfoot or valgus foot is a multifactorial deformity that results from several structural changes of the foot anatomy, leading to a misalignment of the foot and ankle joints. Such alterations cause pain and potentiate the alteration of the foot biomechanics. Statistics estimate that its prevalence is about 25% in general population, with females and individuals with higher body mass index and larger feet, being the most affected. It can be easily understood that flatfoot is a pathology that strongly influences the quality of life, not only in a daily basis but also in terms of sports performance, since it increases injury risk. Moreover, recent studies demonstrate the existence of a greater propensity in developing other types of lower limb injuries in individuals with valgus foot [1].

In recent years, adult acquired flatfoot deformity (AAFD) has become a clinical research issue, mainly due to the increasing prevalence of this pathology but also because of the variability of current available treatment alternatives. This variability is caused, in part, by a still latent lack of knowledge of certain biomechanical variables that have not been adequately evaluated by experimental trials. The degree of correction of each treatment is based on the clinicians' empiric experience, which makes the process highly subjective [2] .

The treatment of flexible flatfoot deformity, at an early stage of the disease, undergoes non-surgical treatment, whereas in more advanced stages, surgical treatment, namely osteotomies, are the most indicated [3]. Choosing the best suited osteotomy, while providing an efficient and accurate restoration of the foot biomechanics and functions, has been a troubling subject amongst the medical community.

Having pointed such factors and constraints, this work is presented as a first approach, using Finite Element Method (FEM), for the evaluation of the biomechanical behaviour of the foot when its anatomy sets up in a deformed situation, in this case, the valgus foot. For that purpose, a finite element (FE) model of the foot and ankle with and without deformity is developed to compare the biomechanics of both situations.

The development of FE models that are clinically applicable can be of great use in clinical practice once they can lead the way for novel diagnostic techniques and novel methods for treatment planning/optimization.

1.2. Thesis Outline

The information provided by this thesis is organized in five chapters. In Chapter 1 a brief introduction and motivation for this work is presented as well as its objectives.

Throughout Chapter 2 the anatomical and biomechanical characteristics of the foot and ankle complex are going to be described. Additionally, a brief description of valgus foot deformity is presented, foot arch stability is assessed, and some diagnosis procedures and treatment options are portrayed. The final section of this chapter includes a literature review of previous work on this subject.

The detailed methodology and computational work are described in Chapter 3. This includes the modelling of the foot and ankle complex and the development of the FE model, namely, the definition of material properties, interactions, loads and boundary conditions, as well as mesh generation.

The Chapter 4 comprises the complete FE analysis results of the models in study. Moreover, the more relevant outcomes are discussed based on the biomechanical differences between the two models.

The last chapter of the document is Chapter 5, which includes the main conclusions of the work developed, its limitations and suggestions for future work.

Chapter 2

Background

This chapter aims to describe the anatomical and biomechanical features of the foot and ankle, as well as the characterization of flatfoot from the etiological point of view, its diagnosis and treatment. In addition, a review of previous works involving the modelling of the foot and ankle and its application on the FEM is carried out.

2.1. Terminology

To successfully describe the movement of any biomechanical system, it is mandatory to know the right terminology, that accurately identifies the position and direction of the system under study.

2.1.1. Anatomical Reference Position

In order to perform an accurate description in anatomy, it is necessary to include a reference position. For this purpose, an anatomical reference position was defined, in which the individual is positioned in an upright position, facing the observer. The feet are slightly apart and the upper limbs relaxed on both sides of the body, having the hands facing forward and fingers extended and joined with the thumb located laterally and the head without any inclination [3].

2.1.2. Anatomical Reference Planes and Axes

The human body can be divided into three anatomical reference planes, perpendicular to each other and intersecting at a single point called the centre of mass or centre of gravity of the body. The sagittal plane splits the body vertically by the middle of the spine in two portions: right and left, also providing the notions of medial and lateral. The coronal or frontal plane divides the body into anterior or ventral and posterior or dorsal portions. The axial or horizontal plane splits the body into superior and inferior [3],[4].

To each of these planes there is a perpendicular axis: the frontal or mediolateral axis, perpendicular to the sagittal plane, the anteroposterior or sagittal axis, perpendicular to the coronal plane and the longitudinal axis, perpendicular to the axial plane. Consequently, the rotation in each of the three planes occurs along the respective axis [3].

In the same way that these axes are applied on the human body to describe its movements they can also be applied to any other anatomical structure, particularly to the foot and ankle complex.

All the above information is outlined in *Figure 1*.

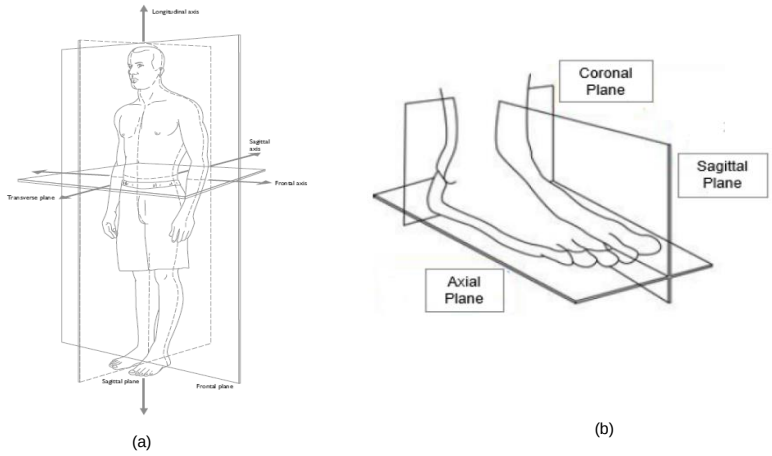

Figure 1 – Anatomical reference planes and corresponding axis (a) applied to the human body and (b) applied to foot and ankle complex. (Adapted from [3],[5])

2.1.3. Motion Terminology

One can consider two forms of pure motion: the linear motion, related with translation and the angular motion, associated with rotation. Overall, human body movements result from a complex combination of these two basic forms of motion but, for analysis purposes, it is easier and more useful to decompose the movements into their linear and angular components [3].

Considering the anatomical reference position, it is assumed that all the body segments are positioned at 0 degrees. Thus, the rotation of any body segment in relation to the anatomical reference position is named according to the movement direction and quantitively defined as the angle between that body segment and the anatomical reference position [3].

The movements occur in the three anatomical planes or in planes with a diagonal orientation to these. As in any other human body structure, movements of foot and ankle can also be identified in the three anatomical planes [3],[5].

In the sagittal plane dorsiflexion and plantarflexion can occur (*Figure 2 (a)).* Dorsiflexion is the flexion of the ankle, where the toes are brought towards the anterior part of the lower limb. In the other hand, plantarflexion is the movement contrary to the latter and concerns the extension of the ankle, causing the separation between the toes and the lower limb. In the axial plane, two fundamental movements are recognized: abduction and adduction (*Figure 2 (b))*. The first is associated with the distal part of the foot away from the midline of the body, while the second corresponds to the approach of the distal part of the foot towards the midline of the body. In the coronal plane, eversion movements are observed, in which the calcaneus is rotated outwards and upwards (*Figure 2 (c))*. In addition to these movements, more complex movements involving the 3 anatomical planes simultaneously can also be

observed, namely, pronation and supination (*Figure 2 (d)*). Pronation is a combination of abduction, eversion and dorsiflexion that causes excessive internal rotation of the foot and ankle. On the other hand, supination is a combined movement of adduction, inversion and plantarflexion where excessive external rotation of the foot and ankle is observed. [3],[5].

Figure 2 - Movements of foot and ankle (a) in the sagittal plane: dorsiflexion and plantar flexion, (b) in the axial plane: abduction (left) and adduction (right), (c) in the coronal plane: eversion (left) and inversion (right) and (d) involving the 3 anatomical reference planes: pronation (left) and supination (right). These figures represent right foot (Adapted from [3])

2.2. Foot and Ankle Anatomy

The foot considers the extension of the lower limb distal to the ankle joint. Besides being the contact point between the body and the ground, it is responsible for providing a stable platform for the upright position [6]. Additionally, it plays a significant role in adapting to uneven terrain, as well as absorbing forces [3]. A set of bones, muscles, joints, and ligaments contribute to the structure of the foot and ankle, which will be described in detail throughout this section.

2.2.1. Bones

Consisting of 26 bones [3], the foot structure is organized into three groups: the tarsal bones which form the skeletal framework for the ankle, the metatarsal bones and the phalanges, which are the bones of the toes [6].

The tarsus is constituted by 7 bones that are organized in a posterior and an anterior group. The posterior group consists of the talus and the calcaneus, while the cuboid, the navicular, the lateral cuneiform, the intermediate cuneiform, and the medial cuneiform form the anterior group. Between these two groups there is an intermediate bone called navicular [3],[5].

Talus is an intercalated bone located superiorly to the calcaneus and supported by it. It is part of the ankle joint due to being articulated with the fibula and tibia. In addition, it also articulates with the navicular bone in the medial part of the foot [5],[6]. It is responsible to support the body weight, which is received by the tibia and transmitted, evenly, to the calcaneus and the anterior part of the foot [8].

The largest and strongest bone of the foot is the calcaneus bone, with an irregular and rectangle shape [7]. It transmits the body weight from the talus to the ground and forms the bony framework of the heel posteriorly [5],[7]. The calcaneus projects forward to articulate with the cuboid on the lateral side of the foot [6].

The intermediate tarsal bone is the navicular, which is a flattened boat shaped bone located in the medial side of the foot, between the head of the talus and the three cuneiforms. It articulates behind with the talus as well as with the distal group of the tarsal bones in front and on the lateral side [3],[5],[7].

Cuboid is a wedge-shaped bone intercalated between the calcaneus and the base of metatarsals 4 and 5, giving support to the lateral cuneiform [7]. It articulates posteriorly with the calcaneus, medially with the lateral cuneiform and anteriorly with the bases of the two lateral metatarsals bases [4],[6].

There are three cuneiform bones: lateral cuneiform, intermediate cuneiform and medial cuneiform [6], located between the navicular proximally, the first three metatarsals distally and the cuboid laterally [7]. The medial cuneiform, in its posterior surface articulates with the navicular and in its anterior surface with the base of the first metatarsal. The intermediate cuneiform articulates anteriorly with the base of the second metatarsal and posteriorly with the navicular. Its medial surface establishes articular contact with the medial cuneiform and its lateral surface with the lateral cuneiform. The lateral cuneiform articulates proximally with navicular, laterally with cuboid, distally with the third metatarsal and medially with the intermediate cuneiform [5],[6].

Five metatarsal bones constitute the metatarsus, which are numbered 1 to 5 from medial to lateral. Each metatarsal bone is formed by a head in its distal end, an elongate shaft in the middle and a proximal base. The head makes articular contact with the proximal phalange of a toe and the base articulates with the bone of the anterior group of the tarsus [4],[6].

The distal part of the foot is formed by 14 phalanges. Each toe has in its structure three phalanges (proximal, middle and distal), except for the great toe, which has only two (proximal and distal). Just like with the metatarsus, each phalange is formed by a base which articulates with the head of the related metatarsal, a shaft and a distal nonarticular head [4],[5],[7].

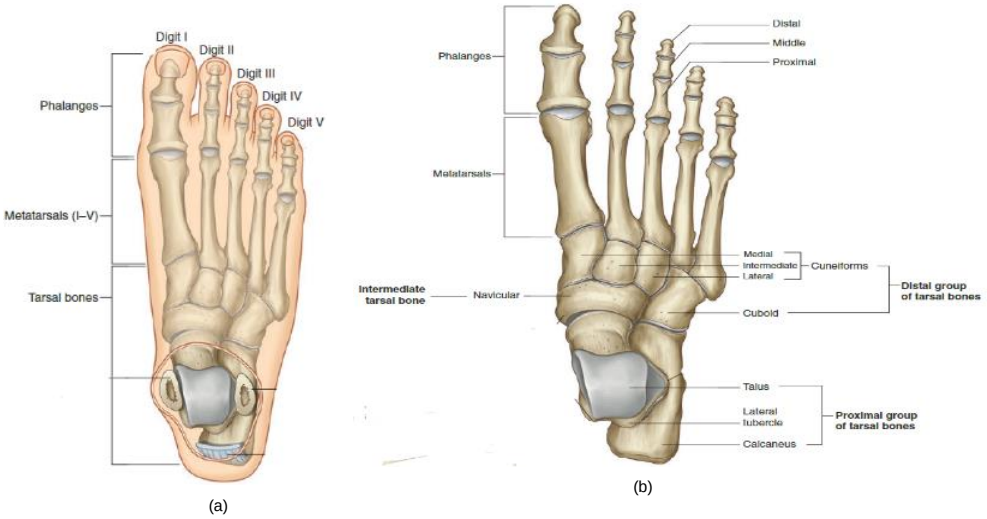

Figure 3 - Foot bones: (a): Division of the foot into the three bony groups (b): Bony structure of the foot. Both figures represent a superiorly vision of the right foot. (Adapted from [6])

2.2.2. Joints and Ligaments

In the foot structure, one can find three groups of joints: hindfoot, that includes the talus and calcaneus; midfoot, formed by the three cuneiforms, the cuboid and the navicular, separated from the hindfoot by the midtarsal joint; and the forefoot, constituted by the metatarsal bones and phalanges that is separated from the midfoot by the tarsometatarsal joint [9].

One can distinguish different joints in the foot, namely, the ankle joint, intertarsal joints, tarsometatarsal joints, metatarsophalangeal joints, and interphalangeal joints. Each of these joints, as well as the ligaments reinforcing them will be described in detail below [6].

The ankle joint is a synovial joint, involving the domed area of the talus and the inferior aspects of the tibia and fibula and includes the distal tibiofibular, tibiotalar and fibulotalar joints. The distal end of the fibula is anchored to the larger distal end of the tibia (tibiofibular joint) by the anterior and posterior tibiofibular ligament, as well as by the interosseous ligaments. The convex surface of the superior talus articulates with the concave surface of the distal tibia, forming the tibiotalar joint, where most motion at the ankle occurs [3], [6].

These three articulations are enclosed inside a joint capsule, with the articular surfaces of the bones covered by hyaline cartilage, and, together, mainly allow hinge-like dorsiflexion and plantar flexion of the foot on the leg [6].

The ankle region is stabilized by the lateral ligaments and by the medial or deltoid ligament. The first can be divided in three parts: the anterior talofibular ligament that attaches the anterior margin of the lateral malleolus to the adjacent region of the talus, the posterior talofibular ligament which runs horizontally backward and medially from the malleolar fossa on the medial side of the lateral malleolus

to the posterior process of the talus and calcaneofibular ligament that is attached above to the malleolar fossa on the posteromedial side of the lateral malleolus and passes posteroinferiorly to attach below to a tubercule on the lateral surface of the calcaneus. On the other hand, the deltoid ligament is formed by an apex attached above to the medial malleolus and a base attached below to a line that extends from the tuberosity of the navicular bone in front to the medial tubercle of the talus behind. Four different parts can be considered on this ligament based on the inferior points of attachment. The more superficial parts are the tibionavicular part that attaches in front to the tuberosity of the navicular bone and the associated margin of the spring ligament and the tibiocalcaneal part, which attaches to the sustentaculum tali of the calcaneus bone. Deep to the tibionavicular and tibiocalcaneal parts there are the posterior tibiotalar part that attaches to the medial side and medial tubercle of the talus and the anterior tibiotalar part which attaches to the medial surface of the talus.

The lateral ligaments contribute to the lateral stability of the joint while the deltoid ligament is responsible for the joint stability on the medial side [3]. Furthermore, the ankle is more stable medially then laterally and this stability increases in dorsiflexion because of the geometry of the articular surfaces involved [9].

All the information presented above its schematized in *Figure 4*.

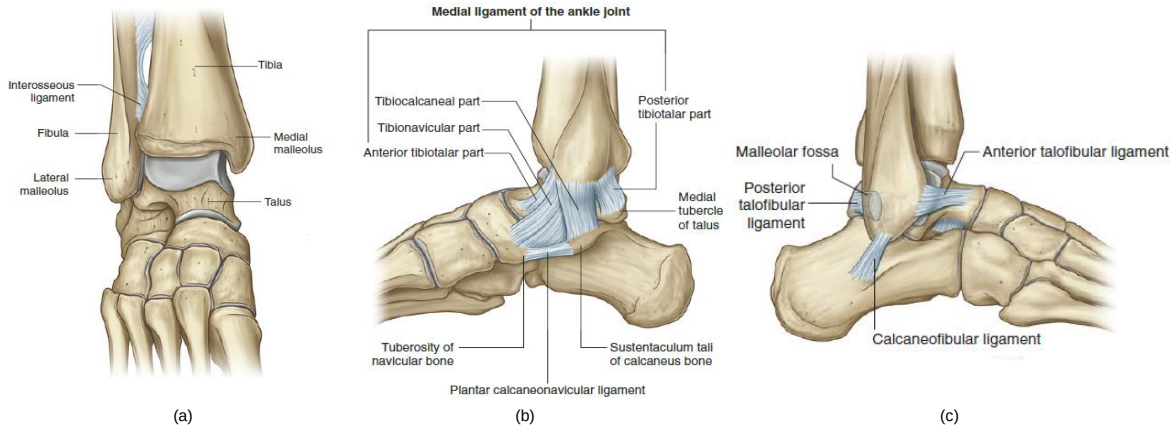

Figure 4 - (a) Anterior view of the ankle joint with the foot plantarflexed, (b) deltoid ligament and (c) lateral ligaments. All the figures represent the right foot. (Adapted from [6])

The intertarsal joints are a set of synovial joints between the individual tarsal bones: subtalar (talocalcaneal), talocalcaneonavicular and calcaneocuboid. These joints mainly allow inversion, eversion, supination and pronation of the foot [6].

The subtalar or talocalcaneal joint lies beneath the talus, involving the plantar aspect of the talus and the superior aspect of the calcaneus. It allows gliding and rotation, which are involved in inversion and eversion of the foot. The stability of the subtalar joint is ensured by three ligamentous groups: the interosseous talocalcaneal, the calcaneofibular and the medial tibiocalcaneal [3], [6] .

The talocalcanealnavicular joint is formed by the articular contact between the head of the talus and the calcaneus and plantar calcaneonavicular ligament (spring ligament) below and the navicular in front. This joint is responsible for gliding and rotation movements, which together with similar movements of the subtalar joint are involved with inversion and eversion. Additionally, it also plays a role in pronation and supination of the foot. The ligaments that contribute for joint stability are the interosseous talocalcaneal, that reinforces joint stability posteriorly, the talonavicular ligament, responsible for superior reinforcement, the spring ligament, which assures inferior joint stability and supports the head of the talus and plays a significant role in resisting depression of the medial arch of the foot in weight—bearing and during walking, and the bifurcate ligament, divided in calcaneocuboid ligament and calcaneonavicular ligament, responsible for reinforcing the lateral part of the joint [3], [6].

The calcaneocuboid joint is a synovial joint that involves the anterior surface of the calcaneus and the posterior surface of the cuboid, permitting sliding and rotation movements involved with inversion and eversion of the foot and also contributes to pronation and supination of the forefoot on the hindfoot. Three ligaments support this joint: bifurcate ligament; long plantar ligament and short plantar ligament (calcaneocuboid) [6].

The intertarsal joints between the cuneiforms and the cuneiforms and the navicular allow limited movement. On the other hand, the joint between the cuboid and the navicular is normally fibrous [6].

The tarsometatarsal joints includes three joints which are distinct anatomically and functionally. They create contact between the anterior group of tarsal bones and the metatarsal bases, allowing limited sliding movements. This joint allows the foot to function as a semirigid unit or to flexibly adapt to uneven surfaces during weight bearing [3], [6].

The metatarsophalangeal joints are ellipsoid synovial joints that establishes articular contact between the heads of the metatarsals with the corresponding bases of the proximal phalanges. Flexion and extension, as well as limited abduction, adduction, rotation and circumduction are permitted within the joint. Additionally, they are reinforced by medial and lateral collateral ligaments and by plantar ligaments [6].

The interphalangeal joints are hinge joints that allow mainly flexion and extension, being supported by medial and lateral collateral ligaments and plantar ligaments [6].

The metatarsophalangeal and the interphalangeal joints are responsible for the toe function to smooth the weight shift to the opposite foot during walking and maintaining stability during weight bearing by pressing against the ground when necessary [3].

Figure 5 represents a schematic view of tarsometatarsal, metatarsophalangeal and interphalangeal joints.

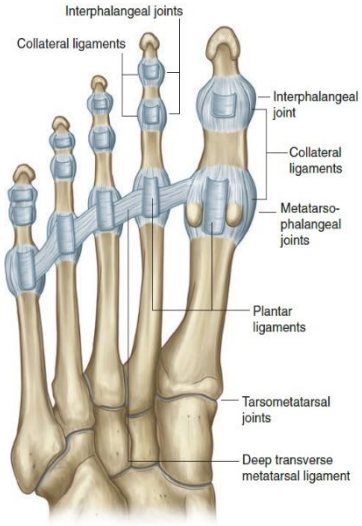

Figure 5 - Tarsometatarsal, metatarsophalangeal, and interphalangeal joints, right foot. (Adapted from [6])

2.2.3. Muscles

The muscles acting on the foot can be divided into two distinct groups: extrinsic and intrinsic. The first group arises from the anterior, posterior and lateral compartments of the leg being mainly responsible for actions such as eversion, inversion, plantarflexion and dorsiflexion of the foot. On the other hand, the intrinsic muscles which are located within the foot are responsible for the fine motor actions of the foot [3], [6].

The intrinsic muscles are situated in the dorsal aspect of the foot or in the sole of the foot. Those on the sole of the foot are organized into four layers: first, second, third and fourth layers [6].

The muscles that constitute the extrinsic and intrinsic groups, as well as their functions, are schematized in *Tables 1* and *2*, respectively.

Table 1 - Extrinsic muscles of foot and ankle complex. (Adapted from [6])

	Muscle	Function
Anterior compartment	Anterior tibialis	Dorsiflexion of foot at ankle joint; inversion of foot; dynamic support of medial arch of foot
	Extensor hallucis longus	Extension of great toe and dorsiflexion of foot
	extensor digitorum longus	extension of lateral four toes and dorsiflexion of foot
	Fibularis tertius	Dorsiflexion and eversion of foot
Lateral compartment	Fibularis longus	Eversion and plantarflexion of foot; supports arches of foot
	Fibularis brevis	Eversion of foot
Posterior compartment	Gastrocnemius	Foot plantarflexion and knee flexion
	Soleus	Plantarflexion of the foot
	Plantaris	Foot plantarflexion and knee flexion
	Posterior tibialis	Inversion and plantarflexion of foot; support of medial arch of foot during walking
	Flexor hallucis longus	Great toe flexion
	Flexor digitorum longus	Lateral four toes flexion

Table 2 - Intrinsic muscles of the foot and ankle complex .(Adapted from [6])

		Muscle	Function
Dorsal Aspect		Extensor digitorum brevis	Extension of toes 2 to 4
		Extensor hallucis brevis	Extension of metatarsophalangeal joint of great toe
Sole	1st layer	Abductor hallucis	Abduction and flexion of the great toe at the metatarsophalangeal joint
		Flexor digitorum brevis	Flexion of lateral four toes at proximal interphalangeal joint
		Abdductor digiti minimi	Abduction of little toe at the metatarsophalangeal joint
	2nd layer	Quadratus plantae	Flexion of toes 2 to 5
		Lumbricals	Flexion of metatarsophalangeal joint and extension of interphalangeal joints
	3rd layer	Flexor hallucis brevis	Flexion of metatarsophalangeal joint of the great toe
		Adductor hallucis	Adduction of great toe at metatarsophalangeal joint
		Flexor digiti minimi brevis	Flexion little toe at metatarsophalangeal joint
	4th layer	Dorsal interossei	Abduction of toes 2 to 4 at metatarsophalangeal joints; resist extension of metatarsophalangeal joints and flexion of interphalangeal joints
		Plantar interossei	Adduction of toes 3 to 5 at metatarsophalangeal joints; resist extension of the metatarsophalangeal joints and flexion of the interphalangeal joints

2.2.4. Foot Arches

There are longitudinal and transverse arches on the foot, formed by the tarsal and metatarsal foot bones, which are responsible for absorbing and distributing downward forces from the body during standing and moving on different surfaces [3], [6]. These arches are interrelated, so failure at one lead to dysfunction at the others.

The posterior end of the calcaneus and the heads of the metatarsals form the longitudinal arch (*Figure 6 (a)*). This arch is divided into its medial part, in the longitudinal arch highest part and lateral side, on its lowest lateral side [6]. The lateral arch is composed of the calcaneus, cuboid bone and 4th and 5th metatarsals. This structure is rigid, and its function is to support body weight. On the other hand, the medial longitudinal arch is formed by the calcaneus, talus, navicular, cuneiform bones and the middle three metatarsals. It is taller and more flexible, which allows it to vary dynamically in shape and configuration during gait. It is mainly supported by the spring ligament and by the plantar fascia [3] [10].

The transverse arch (*Figure 6 (b)*) is highest in a coronal plane that cuts through the head of the talus and disappears near the heads of the metatarsals, where these bones are held together by the deep transverse metatarsal ligaments [6].

Additionally, when muscle tension is present, tibialis posterior muscle also contributes for the support of the foot arches. During weight-bearing there is a deformation of the foot arches and mechanical energy is stored in the stretched tendons, ligaments and plantar fascia as well as in the gastrocnemius and soleus [3].

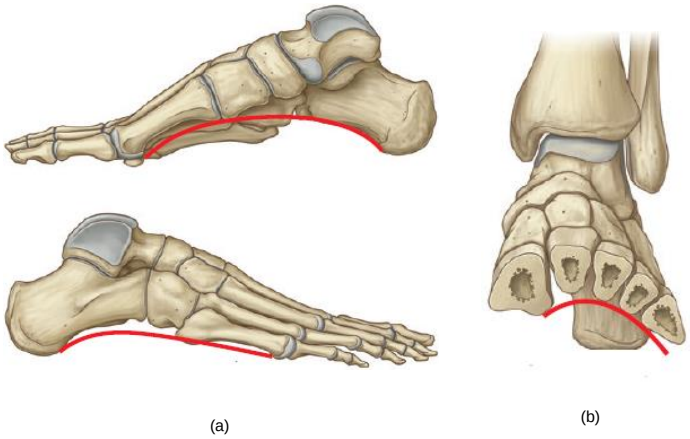

(a) (b)

Figure 6 - Foot arches. (a) - longitudinal arches: medial arch (on top) and lateral arch (on the bottom) and (b) – transverse arch. Both images represent the right foot. (Adapted from [5])

2.3. Valgus Foot

Valgus foot or flatfoot deformity is a complex deformity associated the progressive weakening of the tibialis posterior tendon (TPT) that results in the collapse of the medial longitudinal arch [11], [12]. In the next subsections, the etiology and the classification of this deformity will be described, and an explanation of the diagnosis tools and treatment approaches will be given. Finally, some published finite element foot and ankle models will be presented.

2.3.1. Etiology and Classification

The tibialis posterior tendon is the main responsible for the support of the medial arch of the foot. Once it fails to function, pathologic forces transmitted through the midfoot result in transverse tarsal joint collapse and forefoot abduction. Furthermore, the force vector applied by the Achilles tendon becomes lateral relative to the centre of the subtalar joint, contributing to the valgus deformity seen in patients with valgus foot.

Originally, AAFD was described as tibialis posterior tendon dysfunction, but is now recognized as a progressive deformity that involves many other structures such as spring, deltoid and interosseous ligaments [12].

So, valgus foot is a combination of TPT insufficiency and failure of both capsular and ligamentous structures of the foot. When dysfunction of the spring ligament occurs, it leads to forefoot abduction through the talonavicular and subtalar joint. Therefore, a combination of plantar and medial migration of the talar head leads to flattening of the arch as the foot displaces from underneath the talus. The failure of the interosseous ligament, responsible for connecting the calcaneus and the talus, contributes to heel valgus. In more advanced stages of the disease, the deltoid ligament dysfunction is responsible for a medial ankle instability with ankle deformity. As the deformation progresses, abnormal joint forces could lead to arthritic changes of the hindfoot and midfoot. With that said, flatfoot deformity is the result of the combination of plantar sag, midfoot abduction and heel valgus [11], [13].

Although the main causative factor of flatfoot deformity is recognized to be TPT dysfunction, it was shown to be a multifactorial pathology with other factors contributing to its appearance or aggravation, such as increasing age, obesity, ligamentous laxity, trauma and systemic inflammatory conditions [13]. Additionally, tight gastrocnemius-soleus complex, posterior tendon hypovascularity, diabetes mellitus and hypertension can also contribute to the deformity [12]. Although these are the most common causes of flatfoot deformity, there are some patients that don't demonstrate any known predisposing factor, and yet develop the disease [12].

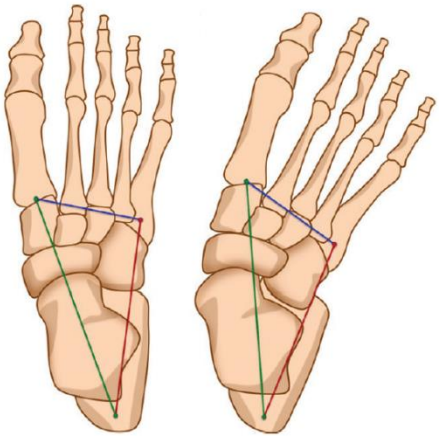

Figure 7 - Alignment of the foot joints in (a) normal foot and (b) flatfoot. The coloured lines represent the arches of the foot. (Adapted from [10])

Johnson and Storm were the first to suggest a classification system for this deformity. This system was a 3-stage system based on the condition of the TPT, hindfoot alignment and flexibility of the deformity. Years later, a fourth stage was added to this classification by Myerson for describing deltoid ligament insufficiency with valgus collapse and degeneration of the ankle. These stages are described in more detail in *Table 3* [12].

Table 3 - Myerson Modification of Johnson and Storm Classification of Adult-Acquired Flatfoot Deformity. (Adapted from [12])

Stage	Description
I	Mild medial pain and swelling with no deformity, can perform heel-rise test but demonstrates weakness on repetition, tenosynovities on pathology with normal tendon length
II	Moderate pain with or without lateral pain, flexible deformity, unable to perform heel-rise test, elongated tendon with longitudinal tears
IIA	<30% talar head uncoverage
IIB	>30% talar head uncoverage
III	Severe pain, fixed deformity, unable to perform heel-rise test, visible tears on pathology
IV	Lateral talar tilt
IVA	Flexible ankle valgus without severe arthritis
IVB	Fixed ankle valgus with or without severe arthritis

2.3.2. Diagnosis

The stage of the deformity influences the clinical presentation of the pathology. In early stages, the patients commonly demonstrate pain over the medial aspect of the foot along the TPT. With the evolution of the disease, the complains are associated with arch collapse and forefoot abduction [12].

In the physical examination, the doctor will observe hindfoot valgus and forefoot abduction from behind if the deformity is present. Additionally, the “too many toes” sign is also indicative of the presence of the disease, being consistent with forefoot abduction [12].

Tenderness, swelling or defects should be identified through palpation along the course of the TPT. Muscle strength and motion about the ankle must also be assessed as well as subtalar mobility for the presence of a fixed deformity [12].

Single and double-limb heel-rise will allow to evaluate the strength of the TPT. If the patient’s manifests an inability to invert the hindfoot or to perform the test, then a tendon dysfunction is present [12].

The gold standard for diagnosing valgus foot is clinical evaluation, but weight-bearing radiographic images are very helpful in the classification of the deformity. The images are acquired from different views: anteroposterior, lateral and hindfoot radiographs. There are several parameters that should be measured in the images to evaluate if the pathology is present by evaluating longitudinal arch flattening, hindfoot valgus and forefoot abduction [12]. For the evaluation of the longitudinal arch the Meary’s angle, the calcaneal inclination angle and the calcaneal-5th metatarsal angle must be used. The most common metrics for hindfoot valgus and forefoot abduction are the talocalcaneal angle, talus-1st metatarsal axis and the talonavicular angle [10].

MRI is also a very important diagnostic tool, due to its high sensitivity and specificity for AAFD, since it allows for a visualization of soft tissues, specifically, the ligaments and tendons, which are the mainly affected in the pathology [12], [13].

Additionally, ultrasonography can also be considered to evaluate the condition of TPT and other similar structures. Tendoscopy, a minimally invasive modality, can also be used to evaluate tendon pathology, especially in symptomatic patients with negative MRI [12].

2.3.3. Treatment

Two types of treatment can be assessed to attenuate or correct the symptoms of valgus foot: the non-operative management and the operative management.

The non-operative or conservative management is commonly used as the first line of treatment for the flatfoot deformity. This type of treatment includes immobilization, nonsteroidal anti-inflammatory drugs, braces, orthotics and physical therapy [12].

In cases where non-operative modalities fail, operative intervention is warranted. The options for surgical treatment are defined by the stage of the deformity [13].

For stage I patients, surgical treatment is very uncommon.

In the case of stage II patients, the surgical treatment involves osteotomies that can be performed individualized or combined with tendon transfer. The flexor digitorum longus transfer to the navicular bone aims to improve inversion strength and oppose the peroneus brevis. This procedure can also help with the correction of abduction deformity through the transverse tarsal joints. However, FDL transfer alone leads to limited deformity correction, this requiring additional bony procedures [13].

A calcaneal osteotomy is commonly used to address hindfoot valgus, with significant results in maintaining the longitudinal arch and protect the medial soft tissue stabilizers from improper stress [12], [13].

Other common procedures performed are Evans procedure for stage IIb patients and an opening wedge medial cuneiform osteotomy is commonly used to correct the deformity of patients in stage IIa [13].

For stage III patients, doctors commonly opt for an arthrodesis since the deformity is no longer passively correctable. This consists in a combination of fusions and corrections involving the subtalar, talonavicular and/or calcaneocuboid joint. In these cases, the functional results are inferior to those expected following operative management for stage II [12], [13].

The surgical treatment for stage IV, deltoid reconstruction can be performed for a flexible deformity if no degenerative alterations were observed but, for a rigid deformity, a tibiocalcaneal or a pantalar arthrodesis seems to be the better option [12], [13].

2.4. Finite Element Foot and Ankle Models

The first biomechanical evaluations of foot function were performed in cadaveric models. From these studies, important information regarding the biomechanics effects of tendons, ligaments and plantar fascia were taken. However, cadaver studies require high financial investments in measurement equipment, as well as a meticulous control over the study samples that guarantees the biomechanical characteristics of the tissue [2]. Moreover, some limitations have been identified, especially when dealing with a certain kind of pathologies which is the case of AAFD. Due to the lack of flatfoot donors, healthy foot samples have been frequently used to artificially create flatfoot deformities by releasing or sectioning ligaments and tendons. However, clinical flatfoot functions are not fully reproduced through these artificial flatfoot samples since they are both patient- and stage-dependent [14]. Limitations of the measurement techniques lead to difficulties obtaining the detailed biomechanics of the inner foot, like the stress distribution in the bones and soft tissue, and the contact pressure at the joints [15].

The development of FE models arises with the capability of surpass some of the limitations inherent to cadaveric studies. FE modelling and analysis has become an increasingly important tool, as computational resources become more powerful, and data handling algorithms become more sophisticated. It has shown to be an effective tool in predicting musculoskeletal function and changes in performance with injury or surgical procedures [16].

Finite element method was first applied to biomechanics field, namely, to skeletal parts, in 1972, in a work developed by Brekelmans et al. [17]. From that moment on, FE publications on biomechanics have grown significantly and, nowadays, there is a huge number of publications regarding FE analysis applied to biomechanics, where different anatomical structures are studied with the most variety of goals.

The need for report the stress patterns of the foot to allow a better understanding and prevention of some diseases such as diabetes and leprosy led to the necessity of develop foot and ankle FE models. The first reported study was published in 1981 [18] , in which a 2D model for the soft tissues of foot's plantar aspect, including muscles, fascia and skin as well as a modelled foam sole was developed with the goal of documenting the stress distribution in the diabetic foot. However, the model didn't contemplate bony structures, as they were only included years later, in 1993, by Patil et al. [19] who developed a simplified foot model to study the regions of high stresses during three different gait cycle positions: mid-stance, heel strike and push-off positions.

The model created (*Figure 8 a)*) included 2D representations of the talus and calcaneus bones combined, the navicular bone and the cuneiform and metatarsal bones also combined.

These two models marked the beginning of FE foot and ankle modelling, but they were very simplified 2D models with a significant lack of complexity. The need to develop more realistic models led to the development of the first 3D foot model in a work conducted by Jacob et al. [20] in 1995. This model used two different arches of the foot including bones, ligaments and cartilages to study the

regions of high stresses during mid-stance phase of walking (*Figure 8 b)*. The medial arch consisted of the talus, navicular, the three cuneiforms, three metatarsals and three toes, whereas the lateral arch included the calcaneus, the cuboid, two metatarsals and two toes. From this study, it was possible to conclude that the ankle joint supports most of the body weight during that period of time.

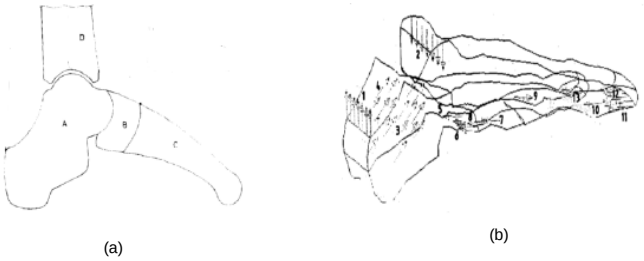

(a) (b)

Figure 8 -(a) Ankle model developed by Patil et al. (Adapted from [15]) and (b) 3-D ankle model created by Jacob et al. (Adapted from [16])

Despite the increase in complexity with the development of a 3D foot model, the existing models still lack complexity both in the anatomical point of view, since several bones were combined, but also from the mechanical point of view, since the ligaments and cartilages were modelled as materials with a linear elastic behaviour, whereas, in fact, they had a non-linear behaviour [21].

The first 3D finite element model of a normal foot structure, including bones, ligaments and cartilages was developed by Gefen et al. [22] in 2000. The goal of this work was to simulate the joint behaviour of discrete moments of the gait cycle. Techniques such as contact pressure display method and digital radiographic fluoroscopy were used to measure *in vivo* the gait cycle, in order to pinpoint the position of the foot as well as the plantar pressure distribution. The von Mises stresses of the bony structures were accurately predicted by this model during 6 phases of the gait cycle.

Five years later, Cheung et al. [23] included in his model bones, cartilages, ligaments and plantar fascia, as well as a soft tissue capsule, modelled using an hyperelastic law, which involved all of the other structures. The evaluation of the plantar pressure and the internal load transfer between bones during standing, were the main focus of this study that aimed to understand the formation of foot ulcers, that occur commonly in diabetic patients. This model, showed in *Figure 9,* was able to predict accurately the plantar stress patterns, which seemed to be concentrated in the heel and in the medial metatarsal head's areas. Additionally, the robustness of the model was validated since the results from this study were in line with the observations of plantar foot ulcers at the medial forefoot and heel regions of diabetic patients.

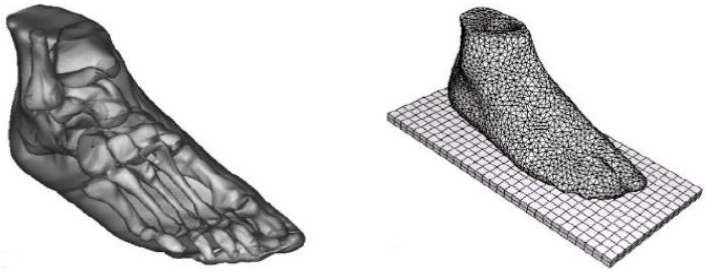

Figure 9 -(a) Bony structure of the model created by Cheung et al. and (b) FE model of the soft tissue capsule. (Adapted from [19])

Most of the papers regarding FE models of flatfoot, simulate the deformity from a healthy subject by releasing some tendons and ligaments.

To the author's best knowledge, the first FE flatfoot reconstructed from data relative to a patient with diagnosed flatfoot was proposed by Lewis [24] in his dissertation. The goal of his work was to develop a procedure for creating 3D subject-specific computational models of the foot for analysing the mechanisms of orthopaedic surgeries with special focus on AAFD.

The foot geometry was reconstructed from CT images of a patient with asymptomatic flatfoot deformity. The FE model was constituted by eleven bony segments: tibia+fibula, talus, calcaneus, navicular, cuboid, medial cuneiform, intermediate cuneiform+2nd metatarsal, lateral cuneiform + 3rd metatarsal, 1st metatarsal, 4th metatarsal and 5th metatarsal. Additionally, 65 ligaments were added to the model was well as a representation of the plantar fascia and a platform simulating the ground.

Several boundary conditions were simulated for the analysis: neutral, inversion, eversion, internal rotation, and external rotation. These boundary conditions were used to simulate standing on different slopes with different amounts of leg rotation. In all simulations a downward vertical force was applied on the tibia and an upward vertical force on the superior-posterior tuberosity of the calcaneus was applied to represent pull of the Achilles tendon.

To adjust the material properties of the ligaments and soft tissue a parameter optimization was used such that the bone movements of the model best matched static positions that were previously measured in RX images of the same subject.

Different surgeries for AAFD correction were simulated: 1st metatarsal-cuneiform arthrodesis, naviculocuneiform arthrodesis, talonavicular arthrodesis, medial column arthrodesis, subtalar arthrodesis and a medializing calcaneal osteotomy.

Since the goal of this paper was just the development of a valid model, no stresses and displacements evaluations were made and, this way, the different surgeries couldn't be compared in terms of biomechanical differences and long-term results.

In 2014, Wang et al. [25] developed a FE flatfoot model with the aim to be used in future studies to simulate surgical procedures and further realize tailor-made surgeries for individual patients.

As in the work from Lewis, the bony structure of the flatfoot was obtained from CT images of a patient diagnosed with AAFD. The model contained 17 bones, 62 ligaments, 9 tendons and the plantar fascia and was validated using a pressure platform system for measuring plantar stress distribution.

The results found that the high stress areas appeared in the rearfoot, midfoot and forefoot in the simulation but were mostly concentrated in the rearfoot area in the measurements. Additionally, the peak stresses were found to be in a range of the peak stresses reported for healthy feet but smaller than those published for flatfoot.

In the next year, Wang et al. [26] proposed a FE model for flatfoot consisting of 27 bone segments, 63 ligaments, plantar fascia and an encapsulated soft tissue for use in surgical simulations to improve individualized treatments. The bones and the encapsulated soft tissue were reconstructed from CT images and the ligaments and plantar fascia were added manually to the model. A ground plate was also added to the model to simulate the ground effect.

In this work, three simulations were performed: a normal balanced standing scenario before surgical correction, a surgical correction of medializing calcaneal osteotomy and a surgical correction of lateral column lengthening.

The results obtained for the balanced standing showed larger stresses at the talonavicular, naviculocuneiform, 1st metatarsal and metatarsal-phalangeal joints for the skeleton and larger stresses in the hindfoot area under the heel and in forefoot under the sesamoid bone for the plantar tissues.

Comparing the results from the balanced standing with the ones obtained for the medializing calcaneal osteotomy, the latter showed an alleviation of the stresses around the talonavicular joint. Additionally, a shift from medial to lateral of the higher stresses was observed. Regarding the plantar tissues, a large amount of stresses was still present under the heel area and an increased on the stresses on the distal areas of 4th and 5th metatarsals was observed. However, stresses at the midfoot were slightly reduced.

Regarding the lateral column lengthening surgery, the simulations showed an alleviation of the stress distributions around the talonavicular joint and a shift of higher stresses from medial to lateral as in the case of the medializing calcaneal osteotomy.

Comparing the results of the two simulated surgeries, lateral column lengthening showed a more significative relief of stress around the talonavicular joint and shifted more stress around the 2nd and 3rd metatarsal bones than medializing calcaneal osteotomy. On the plantar tissues, lateral column lengthening also showed a more significant shift from medial to lateral.

Chapter 3

Methods

This chapter describes the steps involved in the development of the 3D FE models of the foot with and without deformity. In particular, the steps followed the generation of the geometry, including the bones, the cartilages and the ligaments, the process of assembling all the parts and the creation of the FE models of both the healthy and the deformed foot. The definition of material properties, interaction between the parts, loading and boundary conditions and mesh generation are included in the creation of the FE models.

3.1. Image Acquisition and Segmentation

The process of developing a 3D FE model of any anatomical structure starts with the acquisition of the medical image that will be used to define the three-dimensional geometry of the tissues involved. In this case, weight-bearing CT images were used to obtain the geometry of the bones. These type of CT has shown to be more accurate compared with conventional CT in demonstrating pronounced deformity and increased valgus in flatfoot patients since it shows the bone relationship in standing physiological load [27] . This technique has been reported to be useful for the evaluation of flatfoot deformity and associated complications [28] as well as preoperative planning. It is important to point out that these images were acquired by the only equipment available for this purpose in Portugal.

A weight-bearing CT of a left foot of a 44-year-old male with healthy feet was used to obtain the geometry of the foot without deformity and a weight-bearing CT of a right foot of a 58-year-old female diagnosed with AAFD was used to obtain the geometry of the flatfoot. The segmentation of these images was performed in the open source software ITK-SNAP (version 3.8.0, 2019) [29], which allows the navigation through medical images, the manual delineation of anatomical regions of interest (ROI) and to perform semi-automatic and manual image segmentation.

Since medical images contain, not only information relative to the human body, but also unwanted signals such as artifacts or blurred edges [30], three techniques are used to perform bone segmentation: global thresholding, active contour and manual segmentation. ITK-SNAP implements the active contour method for the segmentation, a semi-automatic approach which combines the efficiency and repeatability of automatic segmentation with human expertise, since the user must specify the initial contour, balance the various forces which act upon it, as well as monitor the evolution [29]. In this technique, the evolving contour is represented by a closed surface which has physical properties and deforms, adapting to the image features, under internal or external mechanical forces. These forces are

calculated iteratively and, while internal forces modulate evolution based on the contour's geometry, external forces incorporate information from the image being segmented [31].

For this work's purpose, the .DICOM files from the weight-bearing CT of the healthy and flatfoot were imported to ITK-SNAP and an automatic contrast adjustment was performed in order to emphasize the difference between the bone and the non-bone tissue.

The first step was to define segmentation labels that will identify, with different colours, the anatomical regions in which the segmentation will be performed. In this case, five labels were created, counting with the clear label which is automatically set by the software. The defined labels are showed in *Figure 10* as well as the colours that identify them in the segmentation. Note that the forefoot and midfoot bones were merged into one single label (label 5) because the boundaries between these bones were almost imperceptible. Moreover, the joints in these regions don't allow much movement being limited to flexion and extension and also allow some limited abduction [3],[6].

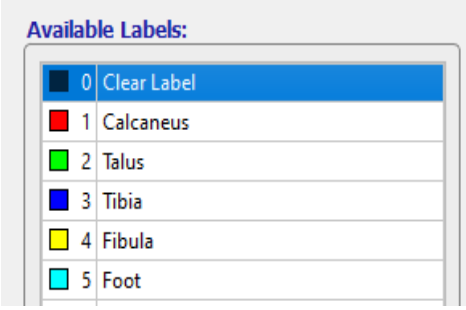

Figure 10 - Labels used to identify different regions on the segmentation.

The next step was to define a ROI, containing only the structure which is going to be segmented. This region is identified by a dashed red rectangle and can be adjusted in all the three anatomical views (*Figure 11*).

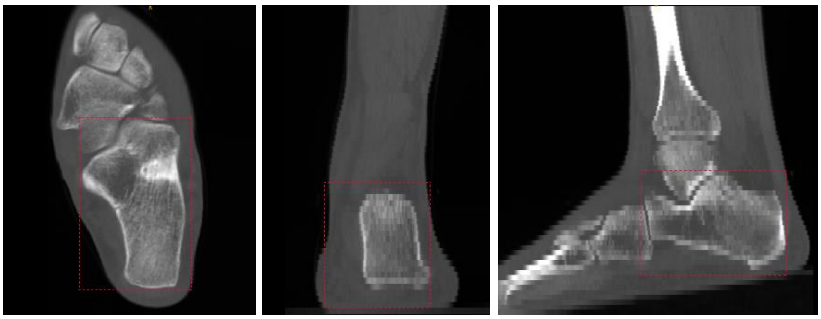

(a) (b) (c)

Figure 11 - ROI (in red) for the active contour segmentation of the calcaneus bone: (a) axial view , (b) coronal view and (c) sagittal view

After defining the ROI, an interface is presented where the input image must be converted into an image that is bright in the regions where the contour should expand, dark in the regions where it should be still and bright blue in the regions where it should retract [31].

The segmentation is initialized by placing one or more spherical “seeds” in the previously defined ROI. Usually, multiple seeds are placed in the structure so that they merge into a single contour during evolution [29]. During evolution the contour expands into the desired regions according to the mathematical equations of the active contour method. Additionally, a visualization in 2D slides and 3D is provided in real-time, allowing the user to stop evolution and reinitialize it if necessary [32]. After this process, a 3D sagittal image of the segmented structure can be seen in the 3D viewer.

Figure 12 illustrates the steps described above for the segmentation of the calcaneus bone. These steps should be repeated for the other labels of the segmentation until the desired 3D model is obtained.

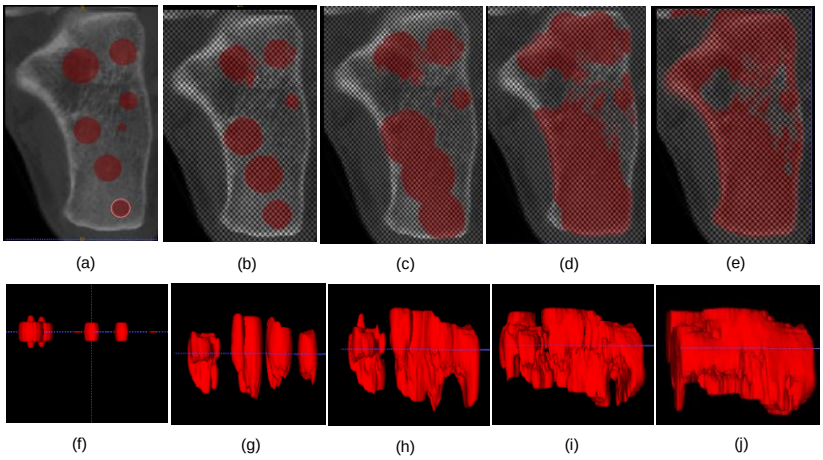

Figure 12 - Axial view of the evolution of the active contour method of the calcaneus bone for (a) t=0, (b) t=50, (c) t=100, (d) t=200 and (e) t=400 and sagittal view of the 3D evolution of the active contour method of the calcaneus bone for (f) t=0, (g) t=50, (h) t=100, (i) t=200 and (j) t=400.

Given the limitations of CT images regarding the voxel size and the small, but inherent, inaccuracy of the active contour method, a final manual segmentation was carried out. For instance, it was used to include in the model the low-density bone regions of tibia and fibula and to refine some boundaries of the other bones segmented.

The final segmentation of the normal foot is presented in *Figure 13.* When the segmentation is concluded, a surface mesh is generated by ITK-SNAP and imported to MeshLab [33].

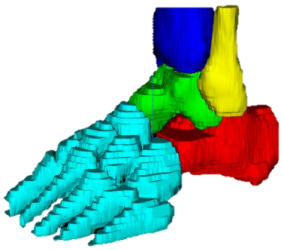

Figure 13 - Final segmentation of healthy foot bones after active contour and manual segmentation methods performed in ITK-SNAP.

The surface mesh exported from ITK-SNAP presents a stair-step shape surface that doesn't correspond to the real surface curvature as well as an excess of nodes and faces that do not express relevant information. For this reason, it was mandatory to take into account an adjustment in the mesh using a smoothing technique. MeshLab was the software used for that purpose since it is a 3D mesh processing system that allows the user to do many operations over the mesh such as applying remeshing filters, mesh cleaning filters, smoothing filters, among other operations [33].

MeshLab displays a variety of smoothing filters in the section "Remeshing, Simplification and Reconstruction Filters" that allow the quality improvement of the mesh by adjusting the nodal coordinates relatively to each other, keeping the mesh topology. The smoothing filter chose to be applied to the foot bones was the Laplacian Smoothening since it is commonly used as an effective filter to amend the stair-step-like artifacts, improving the mesh surface. In *Figure 14,* the results of applying the Laplacian Smoothing Filter to the calcaneus bone can be observed.

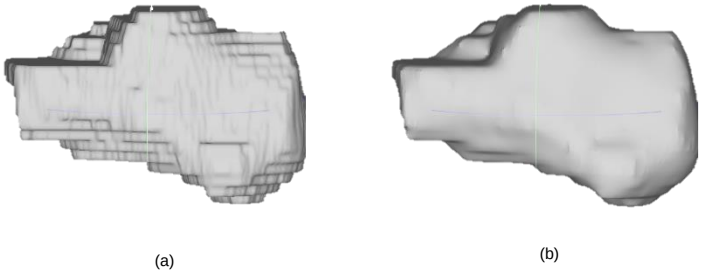

Figure 14 – Imported mesh surface of calcaneus bone of the healthy foot model from ITK-SNAP to MeshLab. (a) without Laplacian smoothing filtering and (b) with Laplacian smoothing filtering.

After repeating this smoothing process for all the bones that compose the foot and ankle structure, it is time to import the surface mesh from MeshLab to SolidWorks® (Student Edition, Academic Year 2020-2021). Some alterations were made in the options regarding import .STL files in SolidWorks® for the bones to be imported as solid bodies. Five solid bodies were imported, corresponding to the five labels created in ITK-SNAP: calcaneus, talus, tibia, fibula and foot (corresponding to the midfoot and forefoot bones).

3.2. Cartilage Modelling

It is true that the cartilages between the foot bones can also be segmented through the same process described before. However, CT scans aren't the image modality most suitable for this purpose since it is almost impossible to distinguish bone tissue from cartilage. MRI images of a foot with and without deformity were also acquired with the aim of being used to segment the cartilages of the model, since it is the most used modality for the direct visualization of articular cartilage. Regardless, the image quality wasn't enough to allow a clear segmentation of the cartilages and, therefore they had to be modelled manually.

Thus, SolidWorks® was used to virtually simulate the cartilages of the model. Five cartilages were modelled: tibio-talar cartilage, connecting the inferior surface of the tibia to the superior surface of the talus; tibio-fibular cartilage, connecting the lateral surface of the tibia and the medial surface of the fibula; calcaneo-talar cartilage, connecting the calcaneus and the talus bone; the last ones were added to make the connection between the calcaneus and the midfoot and forefoot region and the talus and that same region.

Extruded cuts were performed on the surfaces that had irregular geometries in order to facilitate the procedure of adding cartilages. After that, reference planes were created coincidently with these surfaces and the entities were converted in order to make an extruded boss/base [34]. This process allows the creation of a 3D solid from an enclosed surface with a specific thickness. In this case, the thickness was the required to connect the two surfaces of the bodies between which the cartilage was being added.

Figure 15 represents the final 3D foot models after inserting the cartilages, where they are presented in red and the bony structure in grey. These models were exported from SolidWorks® as .parasolid files and imported to ABAQUS® (Dassault Systèmes Simulia Corp., USA).

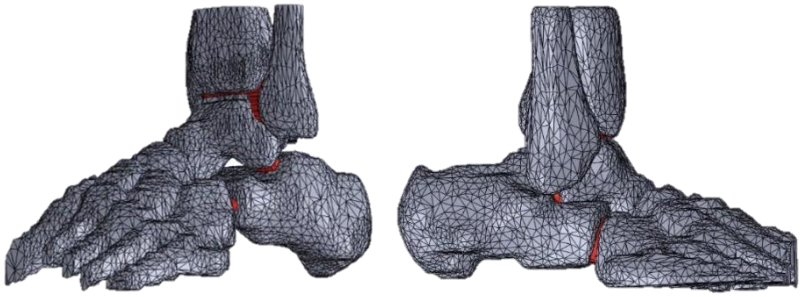

Figure 15 -3D foot models after inserting cartilages with the bones coloured grey and the cartilages in red - (a): normal foot and (b): valgus foot.

3.3. FE Modelling

The .parasolid file of each model was imported to ABAQUS® as individual parts, meaning that each bone and each cartilage was imported as a single part. These parts were named according to the bones and cartilages that they represented. The steps involved in the process of the FE models development will be described in the following subsections.

3.3.1. Ligament Insertion

Given the difficulty of discriminating ligaments and tendons from the surrounding tissue in CT images, they were manually modelled in ABAQUS®.

There are many ligaments and tendons that support the foot and ankle complex but, for this study, only 4 ligaments and 2 tendons were considered since they were the most significant for the pathology according to the literature. Spring ligament (SL), short plantar ligament (SPL), long plantar ligament (LPL) and deltoid ligament (DL) were added to the model. The deltoid ligament can be divided into four individual parts: tibionavicular part (TN), tibiocalcaneal part (TC), posterior tibiotalar part (PTi) and anterior tibiotalar part (ATi). Regarding the tendons, tibialis posterior tendon (TPT) and the Achilles tendon (AT) were modelled. Note that, only the distal part of the Achilles tendon was modelled since the proximal and medial parts were inserted in regions that were not present on the model. The ligaments and tendons added to the model are depicted in *Figure 16.*

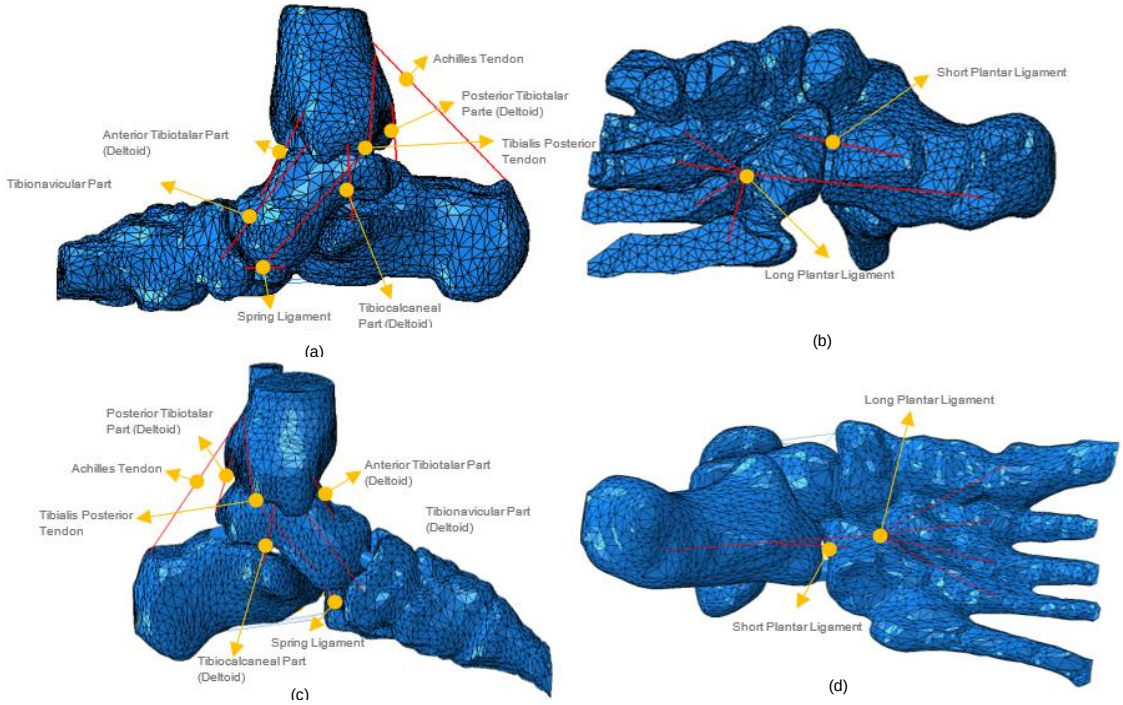

Figure 16 – FE models of the foot and ankle comprising bones, cartilages and ligaments. (a) and (b) normal foot: (a) – lateral view and (b) – plantar view. (c) and (d) valgus foot: (c) – lateral view and (d) – plantar view.

For the modelling of the ligaments and tendons, the first step was to choose the points corresponding to the insertion sites of each structure. These points were carefully chosen based in anatomical images and bibliographic references. Ligaments and tendons differ from each other in the insertion points, since ligaments make the connection between bones and tendons connect muscles to bones. Taking into account that the developed FE models don't comprise muscles, both ligament and tendons were inserted in bones. The coordinates of the insertion points were obtained using a query and then a datum point was created by adding the coordinates of the insertion point. The distance between the points that made up the insertion sites for each ligament/tendon was measured to guarantee that the points would be connected.

The next step was to create a wire part for each ligament/tendon with the right dimension and to create materials regarding ligaments and tendons as well as sections to be assigned for each

structure. These material properties and section assignments are better described in the material properties section. Such structures were modelled as tension only truss elements, using the “no compression” option defined by ABAQUS®. This way, all the parts have their elastic behaviour modified and do not generate tension under compression.

Then, in the assembly module, an instance was created for each ligament/tendon as well as a datum axis using the two datum points previously defined. A parallel edge constraint was used to make the instance parallel to the datum axis and a translation was performed to place it in its right position (coincident with the datum axis). *Figure 17* shows the result of applying this procedure to TPT.

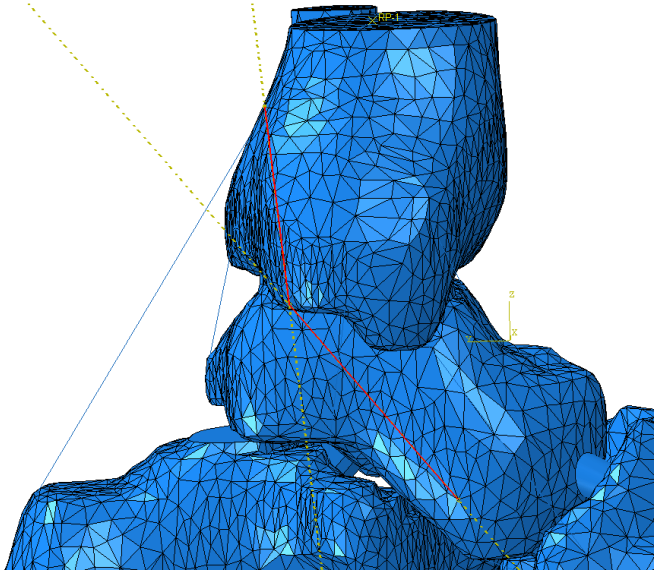

Figure 17 -TPT in its right position after creating a datum axis (dashed yellow lines) with 2 points, applying a parallel edge constraint and translating the tendon to its final position.

In the interaction module, continuum distributing coupling constraints were performed between the datum points that defined the insertion sites and the surfaces where they were inserted in. This was done to ensure that the ligament/tendon is attached to the insertion site and that the forces were uniformly distributed on the surface, mimicking what happens in the human body, while avoiding concentration points.

Additionally, and based on the work of Liacouras et al. [35], a pre-stretch on 2% was applied to every ligament and tendon to represent *in situ* levels. The pre-stretches were added as predefined stress fields in the load module.

3.3.2. Material Properties

The mechanical behaviour of biological tissues is difficult to reproduce in computational models because they are very complex materials, constituted by different cells with different functions and with non-linear material properties. With that said, for the mechanical properties of bone, cartilage, ligaments,

and tendons several approximations had to be considered for the sake of simplicity and to reduce the computational effort.

Bone is known to be a viscoelastic, heterogenous (in terms of mechanical resistance, stiffness and density) and anisotropic material, meaning that it is directionally dependent [36]. However, in this work, it was considered as a linearly elastic, homogenous, and isotropic material, meaning that no difference between cortical and trabecular bone was considered and it is not directionally dependent. A Young's modulus of 7300 MPa was assigned to bone, selected by weighting cortical and trabecular elasticity values [23]. Additionally, a Poisson's ratio of 0,3 was used [34], [37].

Like bone, cartilage has also a viscoelastic behaviour but was considered linearly elastic and isotropic with a Young's modulus of 10 MPa and a Poisson's ratio of 0,4 for its nearly incompressible nature [34], [38].

The ligaments and tendons were also considered as linear elastic materials when, in fact, they present nonlinear elastic behaviour. As said previously, there are some differences between ligaments and tendons and, consequently, they were considered to have different material properties. For the ligaments, a Young's modulus of 264,8 MPa and a Poisson's ratio of 0,4 [39] was used. However, different cross-sectional areas, taken from the literature, were considered for each ligament/tendon. Following the same reasoning, the tendons were also considered to have the same Young's modulus and Poisson's ratio of 1500 MPa and 0,4 [25], respectively and different cross-sectional areas. *Table 4* resumes the material properties of each ligament/tendon as well as the literature references that were used to define them. Note that the cross-sectional area of the plantar ligaments was considered the same since it is very difficult to distinguished them from each other in the measurement trials [40].

Table 4 - Material properties for ligaments and tendons.

Ligament/Tendon	Young's Modulus (MPa)	Poisson's Ratio	Cross-sectional area (mm2)	Reference
Tibialis Posterior Tendon	1500	0,4	16,10	[41]
Achilles Tendon			84,20	[42]
Spring Ligament	264,8		28,48	[40]
Short Plantar Ligament			58,06	[40]
Long Plantar Ligament			58,06	[40]
Deltoid Ligament				
Tibionavicular Part	264,8	0,4	28,08	[43]
Tibiocalcaneal Part			43,20	[44]
Posterior Tibiotalar Part			78,43	[44]
Anterior Tibiotalar Part			43,49	[44]

3.3.3. Model Interactions

The interactions between all parts of the models (bones and cartilages) were considered rigidly bonded using the tool merge geometry, selecting the option retain intersecting boundaries. The interaction between the bones and the ligaments were achieved by using a coupling constraint as explained previously.

3.3.4. Loading and Boundary Conditions

A loading case to simulate a normal standing load position was created with a 375 N descending vertical force, corresponding to half of the body weight of an average individual (75 Kg) leaning on one foot. The load was applied to a reference point (RP) created on the top surface of the tibia and coupled with the top surface of the tibia and the top surface of fibula (*Figure 18*).This allowed an uniform distribution of the load across the surface. This way, a traditional AAFD diagnostic assessment scenario is emulated with the patient leaning on one foot [2].

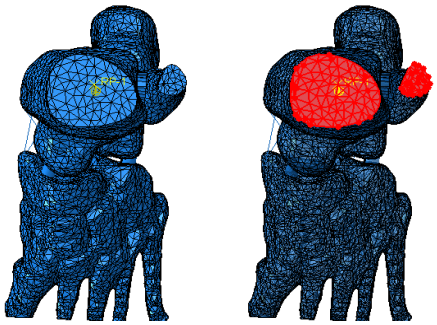

Figure 18 – Loading conditions applied to the normal foot. (a) RP on the top of the tibia surface where the load was applied and (b) Surface (highlighted in red) that was coupled to the RP for distributing the load.

The ground effect was simulated when an adult individual is leaning on one foot. For that purpose, an *encastre* was performed on the inferior part of the calcaneus as well as a blockage of the vertical displacement on the 1st and 5th metatarsals [2], [37]. The defined boundary conditions can be observed on *Figure 19.*

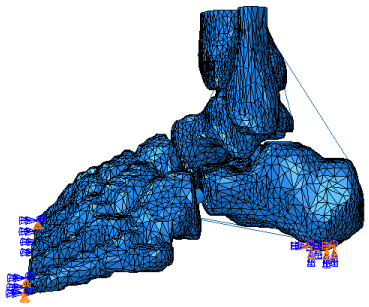

Figure 19 - Boundary conditions applied on the healthy foot.

For comparisons purposes, the same loading and boundary conditions were applied to both foot models.

3.3.5. Mesh Generation

With all the constraints and loads acting on the model defined, the final step before the simulations is the mesh generation. Two 3D options for meshing are provided by ABAQUS®: tetrahedral and hexahedral meshing. Most foot models and biomechanical research make use of tetrahedral elements since they can be more easily automated. However, hexahedral elements seem to have a higher performance in terms of convergence rate and accuracy of the solution [45].

In this work, bones and cartilages were described by linear tetrahedral (C3D4) elements and ligaments were defined by 2-node linear 3D trusses (T3D2).

A convergence analysis was performed to ensure that the FE meshes were computationally efficient but accurate enough. However, this analysis was inconclusive because the model didn't converge. So, the choice of the mesh was made according to the mesh sizes used in the literature, which were in the range of 100 000 – 300 000 elements.

For the merged foot containing the bone and the cartilage a mesh size of 2 mm was chosen for both the healthy foot and the flatfoot. Some adjustments using the virtual topology tool were done in both models to avoid problematic regions on the meshes. Various problematic regions of the mesh identified by ABAQUS® were stored in a set and a seed by edge was performed to these regions with smaller seeds. In the healthy foot a mesh of 270 172 elements was generated, while the mesh generated for flatfoot had 260 864 elements.

The meshing of the ligaments and tendons was done using a linear truss mesh with the size equal to the length of the ligament/tendon to assure that each structure was meshed with only one element. So, the ligaments and tendons were defined with 14 tension-only truss elements.

In *Figure 20* the meshes generated on each model can be observed.

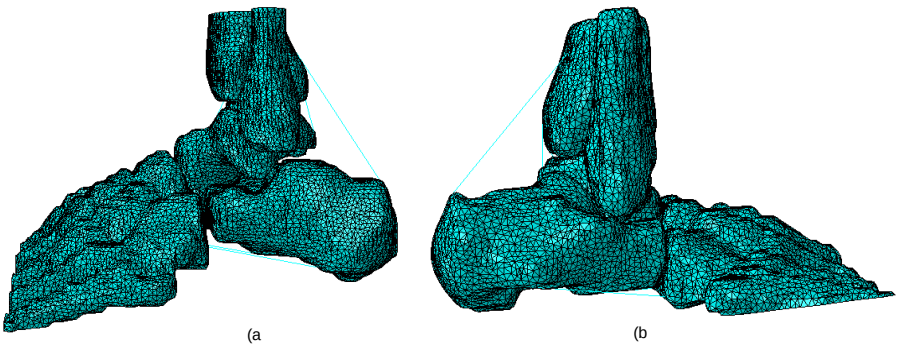

Figure 20 - Meshed foot models. (a) Mesh generated on the healthy foot and (b) mesh generated on flatfoot.

Chapter 4

Results and Discussion

Throughout this chapter, the results of the simulations performed on ABAQUS® will be presented and discussed. The results will be divided into 2 subsections: one regarding bones and cartilages and the other ligaments and tendons. Also, a comparison between the results obtained for the healthy foot and for the flatfoot will be assessed.

4.1. Bones and cartilages

To understand how the stresses are distributed on the foot, von Mises stresses were measured for both the healthy and the flatfoot models. The distribution of von Mises stresses is presented in *Figure 21* for the healthy foot and in *Figure 22* for the flatfoot.

On the superior left size of the figures, a colour scale is displayed, which is organized in ascending order: blue represents low stresses, green represents medium stresses, while orange and red represent high stresses. This scale was normalized to the results of both models be comparable.

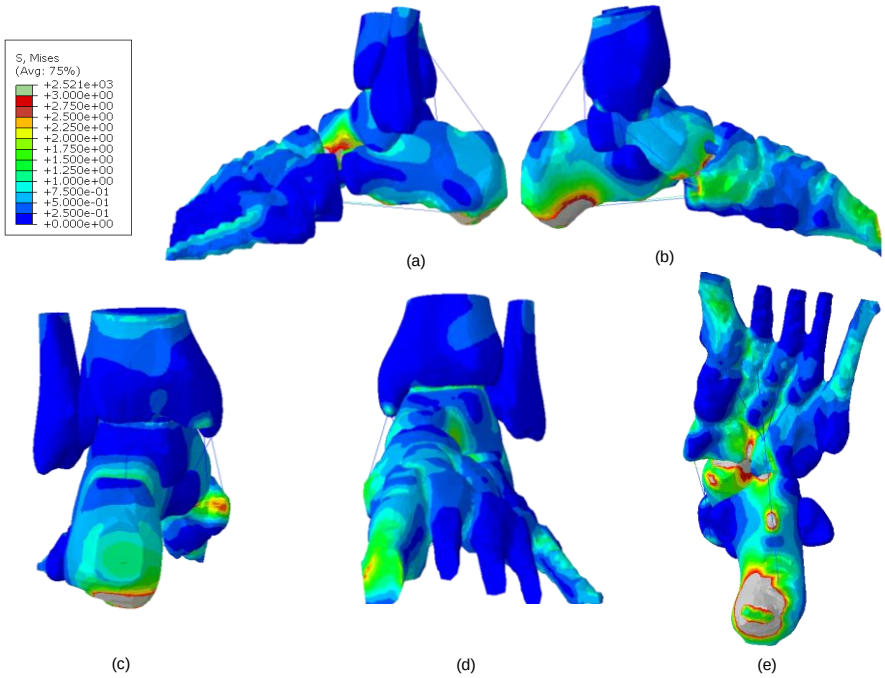

Figure 21 - Von Mises stresses distribution on the healthy foot. (a) lateral view, (b) medial view, (c) posterior view, (d) frontal view and (e) plantar view.

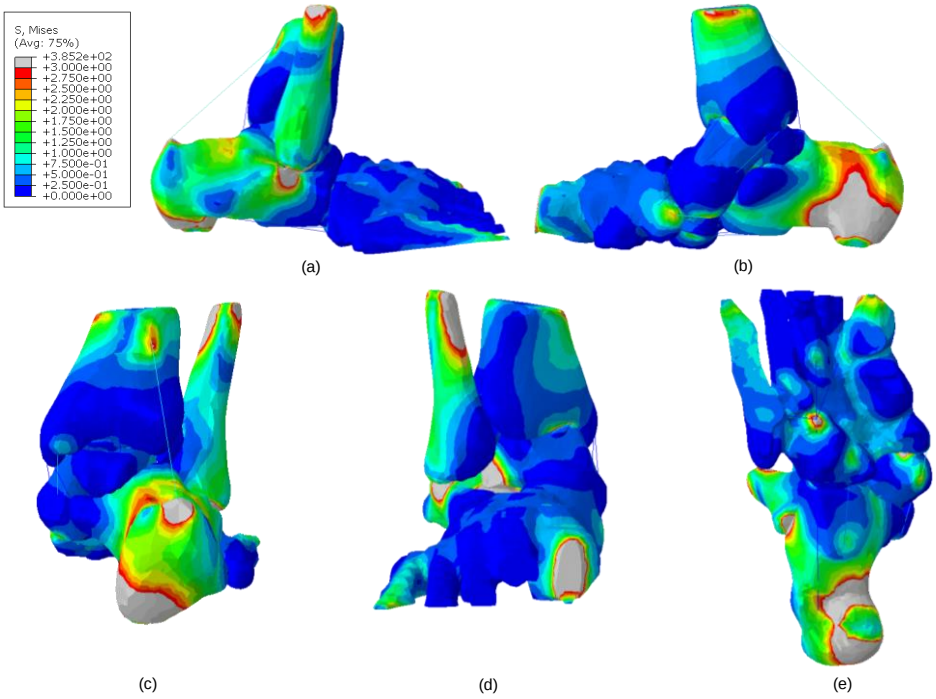

Figure 22 - Von Mises stresses distribution on the flatfoot. (a) lateral view, (b) medial view, (c) posterior view, (d) frontal view and (e) plantar view.

Starting with the results of the von Mises stresses on the healthy foot, one can verify that the higher stress values are in the inferior region of the calcaneus bone and in the frontal region of the talus. On the other hand, the lower stresses occur in the tibia and fibula as well as in the superior region of the midfoot. It is also possible to identify medium stresses regions on the 1st metatarsal.

By analysing in more detail, the plantar aspect of the foot it is possible to verify an accumulation of higher stresses on the calcaneus. The joints of the tarsus are also subject to medium stresses. The same occurs to the 1st and 5th metatarsals. The proximal regions of the 2nd, 3rd and 4th metatarsals as well as the bases of the 1st and 5th metatarsals are the ones with the lower stresses. These results were in agreement with the ones obtained by Wang et al.[46].

Overall, the distribution of von Mises stresses on the healthy foot was the expected. Higher stress regions correspond to regions that contact with the ground in a balanced standing position for a healthy subject [46].

Regarding the flatfoot, one can observe that the higher stress regions occur for almost the same as in the healthy foot: on the inferior part of the calcaneus and on the heads of the 1st and 5th metatarsals. The midfoot continues to be the region with lower stresses. However, an increase on the stresses acting on the tibia and fibula is observed. These bones are the ones that support the load created by the body weight and are responsible for distributing it through the foot. When the geometry of the foot is altered, such as the flatfoot this load transfer is also altered, leading to a different distribution of the stresses within the foot.

On the plantar aspect of the flatfoot, the calcaneus continues to be the bone with higher stresses. However, these higher stresses occupy a bigger area than in the healthy foot. This is because, in the flatfoot, the contact area with the ground is bigger due to the flattening of the arch, and so the stresses distribute differently, across a bigger region. Furthermore, a region with higher stresses is identified in the insertion site of the LPL, probably due to the coupling constraint that was added to guarantee that the ligament was connected to the bone. The proximal regions of the 1st and 5th metatarsals are also subjected to higher stresses because of the boundary conditions applied.

Comparing the von Mises tensions of both models, the main differences are in the von Mises peak tension, with the healthy foot having a much higher value of the von Mises stress. However, this value occurs in a region where bone is in contact with other bone, mainly because of inefficiencies in modelling the realistic geometry of the foot anatomy.

On the plantar aspect of the foot, higher stresses were observed in the flatfoot. As a consequence of the flattened arch, the contact area between the foot and the ground is bigger and so stresses concentrate more in certain regions. This results are in agreement with the ones observed by Wang et al. [47] in his study. Moreover, these higher stress regions occur in both models and correspond to the regions where boundary conditions were applied.

Since the ankle joint is the most significant one in terms of function within the foot mobility, a more detailed evaluation was performed. For that purpose, an individual analysis of the calcaneus, talus, fibula, and tibia was done.

The results of the von Mises stresses distributions for the calcaneus for the healthy and flatfoot are depicted in *Figures 23* and *24*, respectively.

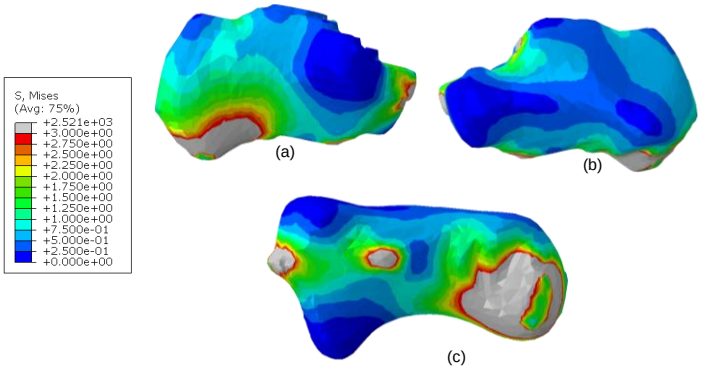

Figure 23 – von Mises stresses on the calcaneus bone for the healthy foot. (a) medial view, (b) lateral view and (c) plantar view.

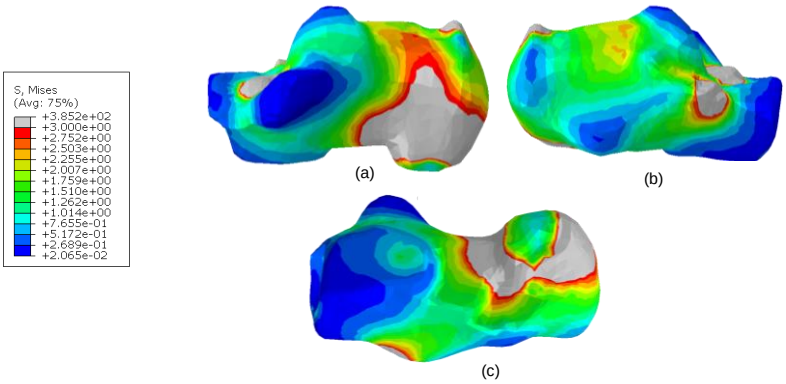

Figure 24 – von Mises stresses on the calcaneus bone for the flatfoot. (a) medial view, (b), lateral view and (c) plantar view.

Visualizing the figures above, some differences are observed between the distribution of the von Mises stresses of both models. Overall, bigger stresses are observed on the flatfoot, especially on the medial and lateral side of the bone. This could be the result of the differences on the load transfer caused by the deformity. On the plantar aspect of the bone, the distribution is relatively similar with the higher stresses occurring on the posterior part, where the boundary condition was applied. However, on the healthy foot, another peak region could be identified corresponding to the insertion point of the long plantar ligament and the zone where the calcaneus and the talus contact each other as a result of geometry limitations.

Regarding the talus bones, the results obtained for the von Mises tensions can be visualized on *Figures 25* and *26*, for the healthy and flatfoot models, respectively.

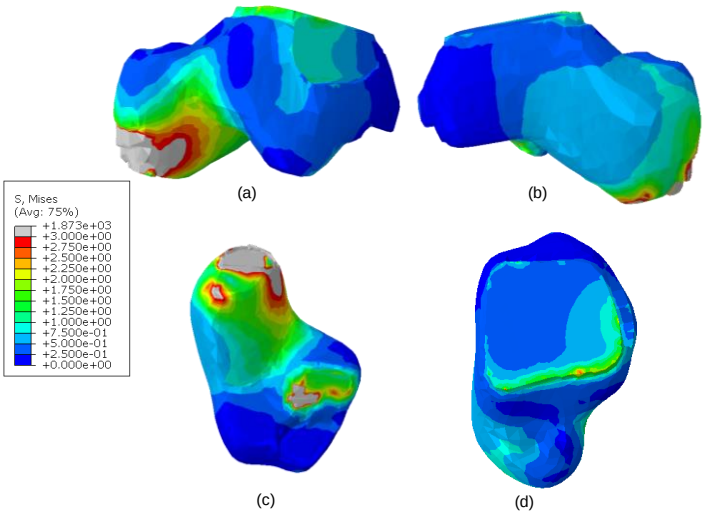

Figure 25 – von Mises stresses distribution on the talus bone for the healthy foot. (a) medial view, (b) lateral view, (c) plantar view and (d) superior view.

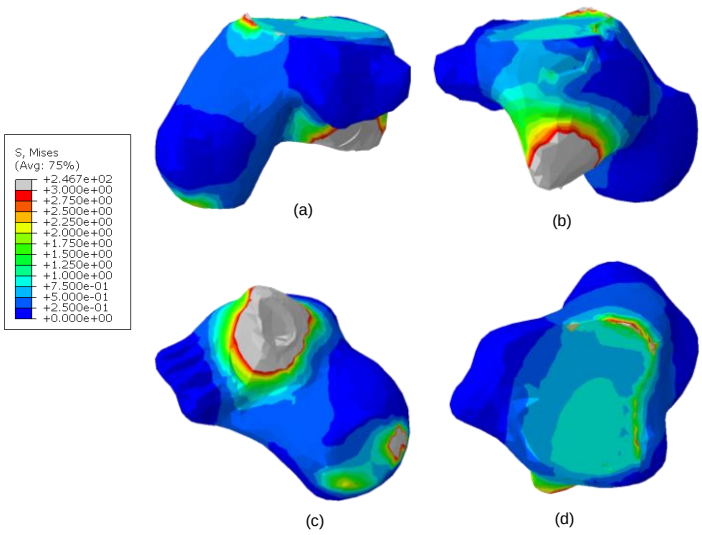

Figure 26 – von Mises stresses distribution on the talus bone for the flatfoot. (a) medial view, (b) lateral view, (c) plantar view and (d) superior view.

Some irregularities on the geometry of the anterior surface of the talus bone of the healthy foot can be observed. This seems to be the cause for the high stress area on this region because such irregularities create a contact zone between the front of the talus and the navicular.

On the lateral side of the bone, higher stresses can be found on the flatfoot in comparison with the flatfoot. In both models, similar stresses distributions occur on the plantar view of the talus.

The superior surface of the talus shows the region where the tibio-talar cartilage connects with the bone. It is possible to observe that, in the flatfoot, a more heterogenous distribution of the stresses occurs. Additionally, an anomaly on the geometry can also be seen on this part of the talus for the flatfoot, which is causing a high stress region.

Overall, the talus of the flatfoot model has higher stress regions but the higher peak of the von Mises tension occurs for the healthy foot.

The tibia of the healthy foot (*Figure 27*), has a much more homogenous stress distribution, while on flatfoot (*Figure 28)*, the stress distribution is much more heterogeneous.

The inferior surface of the tibia corresponds to a contact surface between this bone and the tibio-talar cartilage. One can observe that higher stresses occur for the flatfoot. However, this could be due to the fact that the articular faces have different areas in both models.

The lateral and medial views of the flatfoot show higher stress regions, comparing with the same views of the healthy foot model. Again, these differences are a possible consequence of the misalignment of the foot joints, which leads to an abnormal load transfer.

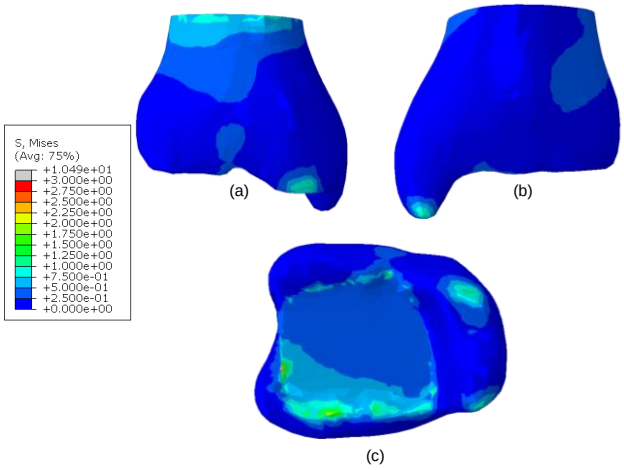

Figure 27 – von Mises stresses distribution on the tibia for the healthy foot. (a) anterior view, (b) posterior view and (c) inferior view.

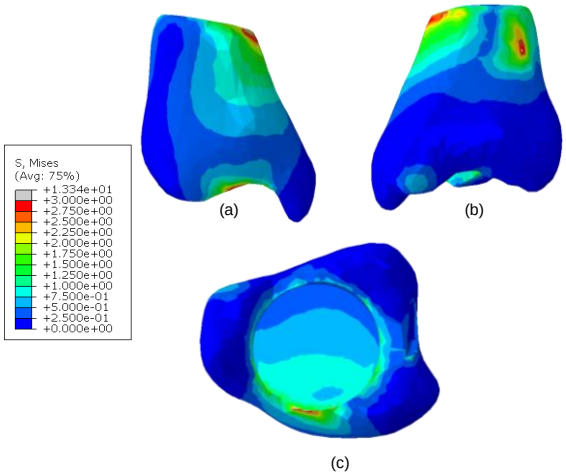

Figure 28 – von Mises stresses distributions on tibia for the flatfoot. (a) anterior view, (b) posterior view and (c) inferior view.

The fibula is the bone with a bigger discrepancy when comparing the healthy foot (*Figure 29)* and the flatfoot (*Figure 30*).

Additionally, higher stresses can be observed on the top surface of the fibula and expand to its medial and lateral parts. Once again, this can be a consequence of the abnormal load transfer that occurs when the foot anatomy sets up on a deformed situation. However, such a big difference wasn't expected, so undetectable abnormalities on the development of the FE model can also be a reason.

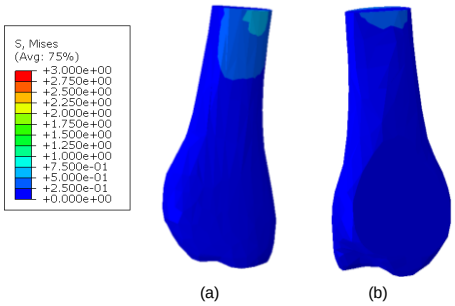

Figure 29 – von Mises stresses distribution on fibula for the healthy foot. (a) lateral view and (b) medial view.

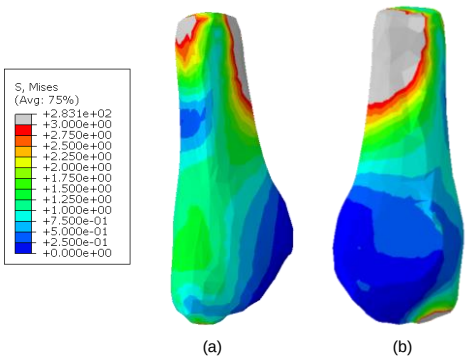

Figure 30 -von Mises stresses distribution on fibula for the flatfoot. (a) lateral view and (b) medial view.

In general, it is possible to conclude that the bones are more loaded when the foot sets up into a flatfoot state, since the load transfer is altered due to the misalignment of the foot joints that characterized the deformity. This alteration on the transfer of the load through the foot joints is responsible for altering the distribution of the stresses within the foot bones and joints. Still, the higher von Mises stresses occur for the healthy foot mainly because of geometry abnormalities on the model.

An analysis of the cartilages was also performed in this study, to see the alterations on this tissue on both models. The peak von Mises stresses on each cartilage were plotted on a graphic that can be seen in *Figure 31.*

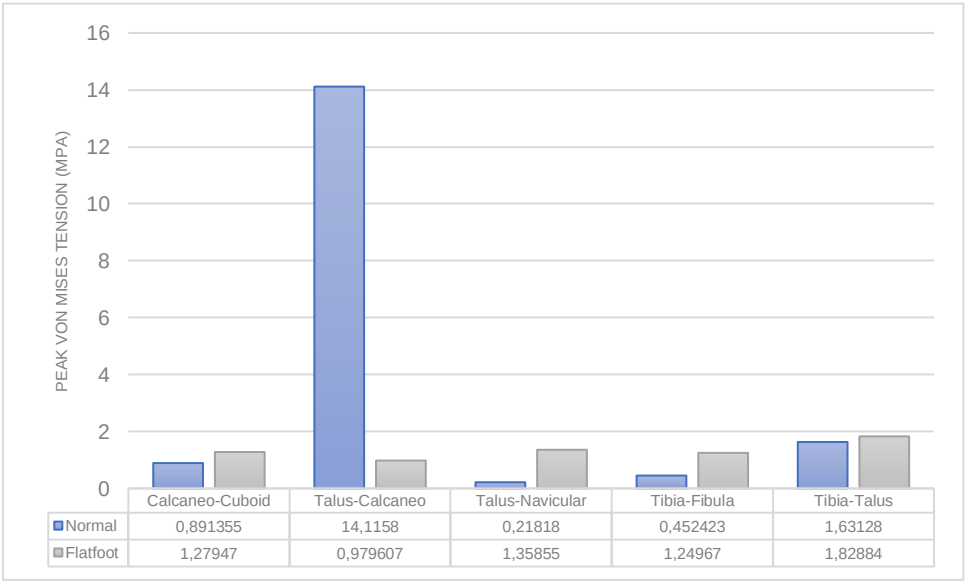

Figure 31 -von Mises peak stresses acting on the cartilages for the healthy foot (blue) and for the flatfoot (grey).

Through the observation of the *Figure 31*, it is possible to verify that an increase of the von Mises peak stresses occur for the majority of the cartilages of the flatfoot, comparing with the healthy foot.

The biggest increase occurs for the cartilage between the talus and the navicular bones. This cartilage has a smaller area on the flatfoot than on the healthy foot and this could be the main cause for this bigger increase.

The increased von Mises peak stress observed for the tibio-fibular cartilage results from the altered load transfer distribution on the flatfoot, that was discussed previously.

The calcaneo-cuboid and tibio-talar cartilages suffer a more attenuated increase on the flatfoot model.

However, the cartilage connecting the talus and the calcaneus bone is the only one that suffers a reduction when comparing the normal foot with the flatfoot. Additionally, this cartilage is the one with the higher peak von Mises stress ($14{,}1158\,MPa$), occurring for the healthy foot. This value is much higher than the von Mises peak stress for the same cartilage of the flatfoot. This discrepancy can be a consequence of model limitations. Probably, this cartilage was modelled with a smaller size than the realistic one. This increases the contact surface between the two bones and leads to a contact between them that probably yields this higher stress value.

4.2. Ligaments and Tendons

As explained previously, ligaments and tendons were modelled as truss elements. A pre-tension was applied to each ligament/tendon to represent *in situ* levels.

Although the ligaments are oriented in space, they are 1D elements and so only an axial load is acting on them.

Note that, some structures, namely the LPL and TPT, must be modelled with different parts to mimic its geometry. In the case of the LPL, the complete ligament is composed of five different parts. Long plantar Ligament 1 corresponds to the truss with the insertion points on the calcaneus and on the cuboid. Long Plantar Ligament 2, 3, 4 and 5 correspond to the bars that connect the cuboid with the 1st, 2nd, 3rd and 4th metatarsals, respectively (*Figure 32 a)*). For the TPT, a similar approach was taken with TPT 1 referring to the bar connecting the two insertion points on the tibia and TPT 2 corresponding to the bar connecting the tibia and the navicular (*Figure 32 b)*).

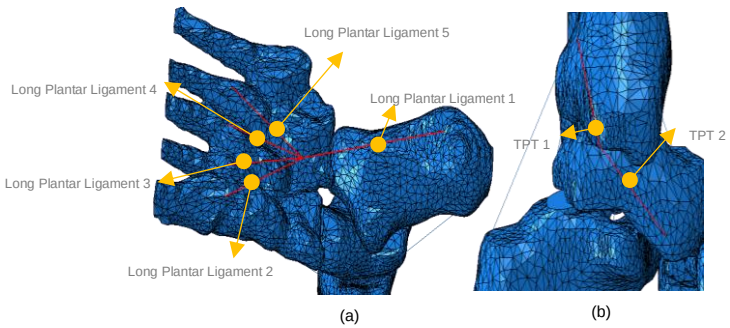

Figure 32 –(a) Long Plantar Ligament divided into its 5 parts and (b) TPT divided in its 2 parts.

In *Figure 33*, the von Mises stresses for each ligament and tendon can be observed for both healthy and flatfoot.

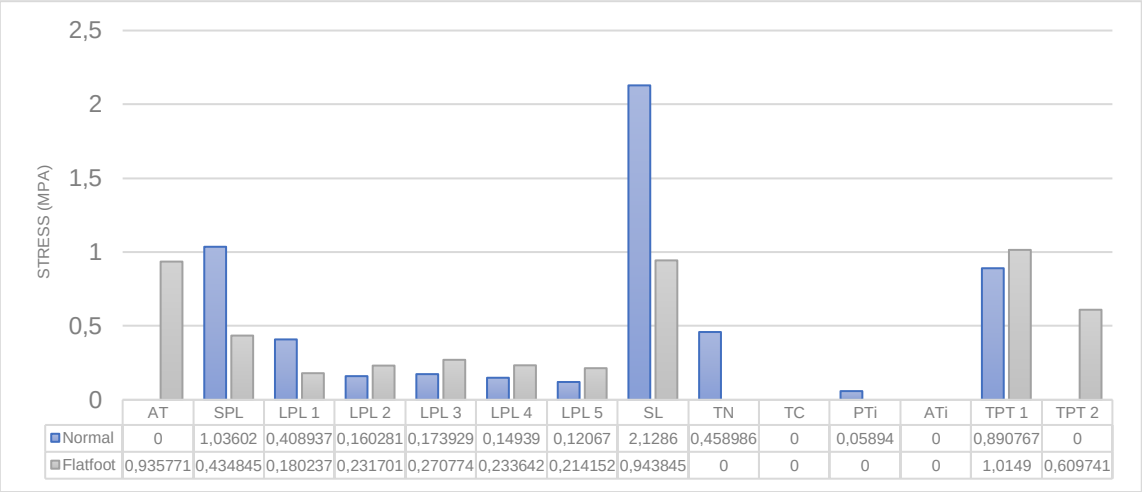

	AT	SPL	LPL 1	LPL 2	LPL 3	LPL 4	LPL 5	SL	TN	TC	PTi	ATi	TPT 1	TPT 2
Normal	0	1,03602	0,408937	0,160281	0,173929	0,14939	0,12067	2,1286	0,458986	0	0,05894	0	0,890767	0
Flatfoot	0,935771	0,434845	0,180237	0,231701	0,270774	0,233642	0,214152	0,943845	0	0	0	0	1,0149	0,609741

Figure 33 – Ligaments and tendons stresses acting on the healthy foot (blue) and on the flatfoot (grey).

By analysing *Figure 34* one can observe that, for AT, LPL 2, LPL3, LPL 4, LPL 5, TPT 1 and TPT 2 there is an increase in tension of the flatfoot compared with the healthy foot. The contrary is observed for the SPL, LPL 1, SL, TN and PTi. The tibiocalcaneal and anterior tibiotalar parts of the deltoid ligaments remain the same in both models.

For the healthy foot, SL is the ligament with the higher value of tension ($2{,}1286\ MPa$) and in the flatfoot is the TPT 1 ($1{,}0149\ MPa$).

The increase in the stresses of most of the ligaments/tendons is expected because, giving the alterations in the geometry inherent to the deformity, one can expect that the ligaments to be subject to higher stress values.

On the other hand, the fact that there was a decrease of the tension on the spring ligament, and since it is one of the most affected on the deformity, one can conclude that it can be already affected on this patient.

Some structures yield 0 stresses values probably because they were compressed instead of stretch, but, since the “no compression” option was chosen this can’t happen on the models. Note that most of these 0 stresses values occur for the TN, TC, PTi and ATi of the flatfoot. These ligaments are part of the deltoid ligament, which is strongly affected by this deformity. As explained for the SL, these values may mean that the DL could be already affected on the patient in study.

Chapter 5

Conclusion

The aim of this study was to create a FE model of both a healthy and a flatfoot that was able to predict, by comparing both models, the biomechanical alterations of the foot when its anatomy sets up in a deformed situation.

A FE model for both a healthy foot and a flatfoot was developed comprising bones, cartilages, ligaments, and tendons. The geometry of the bones was obtained through weight-bearing CT images of a healthy and a diagnosed flatfoot and the boundary and loading conditions were taken from the literature and previous studies to simulate a traditional AAFD diagnostic assessment scenario.

A comparison between the von Mises stresses distribution of the healthy and the flatfoot was done for the entire foot as well as for the individualized bones that made up the ankle joint. Additionally, von Mises stresses of cartilages, ligaments and tendons were also targeted. Overall, the results showed that the flatfoot was subject to higher stresses than the healthy one. However, the peak von Mises stresses occurred for the healthy foot probably due to limitations on the development of the FE model. Concerning the cartilages, it was possible to conclude that the, in the flatfoot the peak von Mises stresses was increased comparing with the healthy foot, due to the altered load transfer provoked by the misalignment of the foot joints that characterized the deformity.

The results obtained in the study of the ligaments and tendons allowed to conclude that the majority of the ligaments and tendons of the flatfoot were more tensioned than the ones of the healthy foot. Additionally, some of them yield 0 stress values, meaning that they could be under compression instead of tension, since the “no compression” option was used. On the other hand, the results obtained for the spring and deltoid ligaments could mean that these ligaments were already affected on the patient studied on this work.

It is important to mention that, to the author’s best knowledge, this is the first FE study on the literature that studies the biomechanical alterations of a flatfoot compared with a healthy foot.

5.1. Limitations and Future Work

This thesis could be the starting point for further investigation about the internal biomechanics of the flatfoot, contributing for a better understanding of the deformity and, consequently, an improvement of the treatment options. Nevertheless, the models have some limitations which should be addressed to create a more outright representation of the foot and ankle complex, thus being able to better represent and reproduce *in vivo* conditions.

The main limitation has to do with the mechanical properties used in this work. This is because bone, cartilage, and ligaments/tendons, were modelled as linear elastic, isotropic and homogenous, when in fact they possess other mechanical characteristics. For more realistic biological conditions, future studies should include a differentiation between cortical and trabecular bone. On the other hand, for the cartilages, ligaments and tendons anisotropic and viscoelastic material properties should be used [48] . Moreover, ligaments and tendons should be modelled with more than one truss since they are composed of multiple collagen fibres and not of one single fibre [6].

A second limitation concerns the loading and boundary conditions used on the work. A balanced standing position was simulated with only the body weight acting upon it. In the future, simulations under different stance phases as well as adding the role of muscles forces could lead to more realistic models and more accurate conclusions.

Another limitation is the fact that the conclusions were taken based on only one AAFD patient. In the future, more patients should be analysed, in different stages of the deformity, to allow a better prediction of the results.

Finally, further investigation is required addressing the limitations described above and, in the future, the model should be used to assess the different treatment options by performing them computationally. This way, the long-term effects on the biomechanics of the foot could be assessed and, hopefully, this work will contribute to the development of an optimal surgery plan and a tailor-made surgery for individual patients.

References

[1] S. N. K. K. Arachchige, H. Chander, and A. Knight, “The Foot Flat feet : Biomechanical implications , assessment and management,” *Foot*, vol. 38, no. January, pp. 81–85, 2019.

[2] C. Cifuentes-De la Portilla, R. Larrainzar-Garijo, and J. Bayod, “Analysis of the main passive soft tissues associated with adult acquired flatfoot deformity development: A computational modeling approach,” *J. Biomech.*, vol. 84, pp. 183–190, 2019.

[3] S. Hall J., *Basic Biomechanics*, 7th ed. New York: McGraw-Hill, 2015.

[4] J. A. Esperança Pina, *Anatomia da Locomoção*, 4th ed. Lisboa, 2010.

[5] M. Nordin and V. H. Frankel, *Basic Biomechanics of the Musculoskeletal System*, 4th ed. New York.

[6] R. L. Drake, A. W. Vogl, and A. W. . Mitchell, *Gray’s Anatomy for Students, 4th Edition*. 2019.

[7] S. K.Sarrafian and A. S. Kelikian, *Sarrafian’s Anatomy of the Foot and Ankle*, Third. .

[8] K. L. Moore, A. F. Dalley, and A. M. R. Agur, *Anatomia Orientada para a Clínica*, 6th ed. .

[9] S. M. Fox, *Bone and joint disorders*. 2016.

[10] D. V. Flores, C. M. Gómez, M. F. Hernando, M. A. Davis, and M. N. Pathria, “Adult acquired flatfoot deformity: Anatomy, biomechanics, staging, and imaging findings,” *Radiographics*, vol. 39, no. 5, pp. 1437–1460, 2019.

[11] E. Vulcano, J. T. Deland, and S. J. Ellis, “Approach and treatment of the adult acquired flatfoot deformity,” no. Table 1, pp. 6–8, 2013.

[12] M. C. Alley, R. Shakked, and A. J. Rosenbaum, “Adult-Acquired Flatfoot Deformity,” vol. 5, no. 8, pp. 1–11, 2017.

[13] N. A. Smyth, A. A. Aiyer, J. R. Kaplan, C. A. Carmody, and A. R. Kadakia, “Adult-acquired flatfoot deformity,” *Eur. J. Orthop. Surg. Traumatol.*, 2017.

[14] Z. Wang, M. Kido, K. Imai, K. Ikoma, and S. Hirai, “Engineering Towards patient-specific medializing calcaneal osteotomy for adult flatfoot : a finite element study,” *Comput. Methods Biomech. Biomed. Engin.*, vol. 5842, pp. 1–12, 2018.

[15] I. Division, B. Engineering, H. Hom, and H. K. Sar, “Computational Models of the Foot and Ankle for Pathomechanics and Clinical Applications : A Review,” 2015.

[16] K. Hollerbach, A. Hollister, and E. Ashby, “3-D Finite Element Model Development for Biomechanics: a Software Demonstration,” *Sixth Int. Symp. Comput. Simul. Biomech.*, 1997.

[17] R. Huiskes and E. Y. S. Chao, “A survey of finite element analysis in orthopedic biomechanics: The first decade,” *J. Biomech.*, vol. 16, no. 6, pp. 385–409, 1983.

[18] S. Nakamura, R. D. Crowninshield, and R. R. Cooper, “An analysis of soft tissue loading in the foot - A preliminary report,” *Bull. Prosthet. Res.*, vol. 18, no. 1, pp. 27–34, 1981.

[19] K. M. Patil, L. H. Braak, and A. Huson, “Stresses in a simplified two dimensional model of a normal foot - A preliminary analysis,” *Mech. Res. Commun.*, vol. 20, no. 1, pp. 1–7, 1993.

[20] S. Jacob, K. M. Patil, L. H. Braak, and A. Huson, “Three dimensional two arch model of a normal

foot for stress analysis," *IEEE/ Eng. Med. Biol. Soc. Annu. Conf.*, pp. 23–24, 1995.

[21] X. S. Zhang, Y. Guo, and W. Y. Chen, "3-D finite element method modeling and contact pressure analysis of the total knee joint in flexion," *3rd Int. Conf. Bioinforma. Biomed. Eng. iCBBE 2009*, no. Nsfc 10702048, pp. 8–10, 2009.

[22] A. Gefen, M. Megido-Ravid, Y. Itzchak, and M. Arcan, "Biomechanical analysis of the three-dimensional foot structure during gait: A basic tool for clinical applications," *J. Biomech. Eng.*, vol. 122, no. 6, pp. 630–639, 2000.

[23] J. T. M. Cheung, M. Zhang, A. K. L. Leung, and Y. B. Fan, "Three-dimensional finite element analysis of the foot during standing - A material sensitivity study," *J. Biomech.*, vol. 38, no. 5, pp. 1045–1054, 2005.

[24] G. S. Lewis, "Computational modeling of the mechanics of flatfoot deformity and its surgical corrections," no. December, p. 119, 2008.

[25] Z. Wang, K. Imai, M. Kido, K. Ikoma, and S. Hirai, "A Finite Element Model of Flatfoot (Pes Planus) for Improving Surgical Plan," vol. m, pp. 844–847, 2014.

[26] Z. Wang, K. Imai, M. Kido, K. Ikoma, and S. Hirai, "Study of Surgical Simulation of Flatfoot Using a Finite Element Model," vol. 45, pp. 353–363, 2016.

[27] G. C. Kunas, W. Probasco, A. M. Haleem, J. C. Burket, E. R. C. Williamson, and S. J. Ellis, "Evaluation of peritalar subluxation in adult acquired flatfoot deformity using computed tomography and weightbearing multiplanar imaging," *Foot Ankle Surg.*, vol. 24, no. 6, pp. 495–500, 2018.

[28] K. Pilania, B. Jankharia, and P. Monoot, "Role of the weight-bearing cone-beam CT in evaluation of flatfoot deformity," *Indian J. Radiol. Imaging*, vol. 29, no. 4, pp. 364–371, 2019.

[29] P. A. Yushkevich *et al.*, "User-guided 3D active contour segmentation of anatomical structures : Significantly improved efficiency and reliability," vol. 31, pp. 1116–1128, 2006.

[30] N. S. Ribeiro *et al.*, "3-D SOLID AND FINITE ELEMENT MODELING OF BIOMECHANICAL STRUCTURES - A SOFTWARE PIPELINE -," 2009.

[31] P. Yushkevich, J. Piven, H. Cody, and S. Ho, "User-guided level set segmentation of anatomical structures with ITK-SNAP," *Neuroimage*, vol. 31, no. 3, pp. 1116–1128, 2006.

[32] P. A. Yushkevich, Y. Gao, and G. Gerig, "ITK-SNAP: An interactive tool for semi-automatic segmentation of multi-modality biomedical images," *Proc. Annu. Int. Conf. IEEE Eng. Med. Biol. Soc. EMBS*, vol. 2016-Octob, pp. 3342–3345, 2016.

[33] P. Cignoni, M. Callieri, M. Corsini, M. Dellepiane, F. Ganovelli, and G. Ranzuglia, "MeshLab: An open-source mesh processing tool," *6th Eurographics Ital. Chapter Conf. 2008 - Proc.*, pp. 129–136, 2008.

[34] G. Marta, C. Quental, and J. Folgado, "Computational study of contact patterns in the ankle joint after ligamentous injury Gonc Biomedical Engineering," no. October, 2018.

[35] P. C. Liacouras and J. S. Wayne, "Computational modeling to predict mechanical function of joints: Application to the lower leg with simulation of two cadaver studies," *J. Biomech. Eng.*, vol. 129, no. 6, pp. 811–817, 2007.

[36] J. Y. Rho, L. Kuhn-Spearing, and P. Zioupos, "Mechanical properties and the hierarchical structure of bone," *Med. Eng. Phys.*, vol. 20, no. 2, pp. 92–102, 1998.

[37] C. Cifuentes-de, R. Larrainzar-garijo, and J. Bayod, "Foot and Ankle Surgery Analysis of

biomechanical stresses caused by hindfoot joint arthrodesis in the treatment of adult acquired fl atfoot deformity : A fi nite element study," *Foot Ankle Surg.*, 2019.

[38] C. Xu, M. Li, C. Wang, and H. Liu, "Nonanatomic versus anatomic techniques in spring ligament reconstruction : biomechanical assessment via a finite element model," vol. 5, pp. 5–7, 2019.

[39] D. W. C. Wong, Y. Wang, A. K. L. Leung, M. Yang, and M. Zhang, "Finite element simulation on posterior tibial tendinopathy: Load transfer alteration and implications to the onset of pes planus," *Clin. Biomech.*, vol. 51, no. June 2017, pp. 10–16, 2018.

[40] K. H. Schmidt and W. R. Ledoux, "Quantifying ligament cross-sectional area via molding and casting," *J. Biomech. Eng.*, vol. 132, no. 9, pp. 1–6, 2010.

[41] S. Park, J. Lee, H. R. Cho, K. Kim, Y. S. Bang, and Y. U. Kim, "The predictive role of the posterior tibial tendon cross-sectional area in early diagnosing posterior tibial tendon dysfunction," *Medicine (Baltimore).*, vol. 99, no. 36, p. e21823, 2020.

[42] S. Bohm, F. Mersmann, A. Schroll, N. Mäkitalo, and A. Arampatzis, "Insufficient accuracy of the ultrasound-based determination of Achilles tendon cross-sectional area," *J. Biomech.*, vol. 49, no. 13, pp. 2932–2937, 2016.

[43] J.-F. Zhu *et al.*, "A new ligament cross-sectional area measuring instrument: Design and application," *Chinese J. Tissue Eng. Res.*, vol. 20, pp. 7654–7659, 2016.

[44] C. Mkandawire, W. R. Ledoux, B. J. Sangeorzan, and R. P. Ching, "Foot and ankle ligament morphometry," *J. Rehabil. Res. Dev.*, vol. 42, no. 6, pp. 809–819, 2005.

[45] S. C. Tadepalli, A. Erdemir, and P. R. Cavanagh, "Comparison of hexahedral and tetrahedral elements in finite element analysis of the foot and footwear," *J. Biomech.*, vol. 44, no. 12, pp. 2337–2343, 2011.

[46] Z. Wang, K. Imai, M. Kido, K. Ikoma, and S. Hirai, "FE Modeling of a Flatfoot Deformity for Improving Surgical Planning," *2015 SIMULIA Community Conf.*, no. 1, pp. 1–12, 2015.

[47] Z. Wang, K. Imai, M. Kido, K. Ikoma, and S. Hirai, "A finite element model of flatfoot (Pes Planus) for improving surgical plan," *2014 36th Annu. Int. Conf. IEEE Eng. Med. Biol. Soc. EMBC 2014*, vol. m, pp. 844–847, 2014.

[48] L. A. Setton, D. M. Elliott, and V. C. Mow, "Altered mechanics of cartilage with osteoarthritis: Human osteoarthritis and an experimental model of joint degeneration," *Osteoarthr. Cartil.*, vol. 7, no. 1, pp. 2–14, 1999.